

Something something something physics

Steven Green
of Emmanuel College

A dissertation submitted to the University of Cambridge
for the degree of Doctor of Philosophy

Abstract

This thesis describes the optimisation of the calorimeter design for collider experiments at the future Compact Linear Collider (CLIC) and the International Linear Collider (ILC). The detector design of these experiments is built around high-granularity Particle Flow Calorimetry that, in contrast to traditional calorimetry, uses the energy measurements for charged particles from the tracking detectors. This can only be realised if calorimetric energy deposits from charged particles can be separated from those of neutral particles. This is made possible with fine granularity calorimeters and sophisticated pattern recognition software, which is provided by the PandoraPFA algorithm. This thesis presents results on Particle Flow calorimetry performance for a number of detector configurations. To obtain these results a new calibration procedure was developed and applied to the detector simulation and reconstruction to ensure optimal performance was achieved for each detector configuration considered.

This thesis also describes the development of a software compensation technique that vastly improves the intrinsic energy resolution of a Particle Flow Calorimetry detector. This technique is implemented within the PandoraPFA framework and demonstrates the gains that can be made by fully exploiting the information provided by the fine granularity calorimeters envisaged at a future linear collider.

A study of the sensitivity of the CLIC experiment to anomalous gauge couplings that effect vector boson scattering processes is presented. These anomalous couplings provide insight into possible beyond standard model physics. This study, which utilises the excellent jet energy resolution from Particle Flow Calorimetry, was performed at centre-of-mass energies of 1.4 TeV and 3 TeV with integrated lumi-

nosities of 1.5ab^{-1} and 2ab^{-1} respectively. The precision achievable at CLIC is shown to be approximately one to two orders of magnitude better than that currently offered by the LHC.

Finally, a study into various technology options for the CLIC vertex detector is described.

Declaration

This dissertation is the result of my own work, except where explicit reference is made to the work of others, and has not been submitted for another qualification to this or any other university. This dissertation does not exceed the word limit for the respective Degree Committee.

Andy Buckley

Acknowledgements

Of the many people who deserve thanks, some are particularly prominent, such as my supervisor...

Preface

This thesis describes my research on various aspects of the LHCb particle physics program, centred around the LHCb detector and LHC accelerator at CERN in Geneva.

For this example, I'll just mention Chapter ?? and Chapter ??.

Contents

1. Future Linear Collider Experiments	1
1.1. The International Linear Collider	1
1.2. The Compact Linear Collider	1
1.2.1. Experimental Conditions at CLIC	1
2. The Sensitivity of CLIC to Anomalous Gauge Couplings through Vector Boson Scattering	5
2.1. Motivation	5
2.2. Event Generation, Simulation and Reconstruction	7
2.3. Modelling of Anomalous Gauge Couplings	9
2.4. Data Analysis	13
2.4.1. Jet Finding	13
2.4.2. Lepton Finding	16
2.4.3. Discriminant Variables	18
2.5. Event Selection	19
2.5.1. Pre Selection	21
2.5.2. MVA	21
2.6. Effect of Anomalous Coupling/Fitting Methodology	24
2.6.1. Choice of Fitting Distribution	26
2.6.2. Application Of Anomalous Gauge Coupling Event Weights	27
2.6.3. Determination of Sensitivity	29
2.7. Results	31
2.8. Sensitivity at 3 TeV	35
2.8.1. Pre Selection - 3 TeV	35
2.8.2. MVA - 3 TeV	37
2.9. Optimisation of Jet Reconstruction	37
2.9.1. 3 TeV Optimal Jet Reconstruction	38

A. Pointless extras	41
A.1. Anomalous Gauge Coupling Quartic Vertices Of Relevance in Vector Boson Scattering	41
A.2. χ^2 Contour Plots for Jet Algorithm Optimisation	44
Bibliography	49
List of figures	51
List of tables	53

*“Writing in English is the most ingenious torture
ever devised for sins committed in previous lives.”*

— James Joyce

Chapter 1.

Future Linear Collider Experiments

1.1. The International Linear Collider

1.2. The Compact Linear Collider

1.2.1. Experimental Conditions at CLIC

The CLIC experiment will operate in a unique environment in comparison to previous generations of lepton colliders and this must be properly accounted for to get an accurate measure of the physics potential that CLIC has to offer. The following aspects of the CLIC experiment present the largest challenges to the physics potential for the CLIC experiment:

- The high bunch charge density. The small beam size at the impact point produces very large electromagnetic fields. These fields can interact with the opposite beam particles causing them to radiate photons in an effect known as beamstrahlung. Beamstrahlung acts to reduce the collision energy of the e^+e^- pairs.
- Beam related backgrounds. Beamstrahlung photons can subsequently interact to produce background events that must be accounted for. Dominant backgrounds of this form that cannot be easily vetoed in the reconstruction include incoherent pair production of e^+e^- and $\gamma\gamma \rightarrow \text{Hadron}$.
- Fast readout technology is crucial. The CLIC bunch train consists of 312 bunches with a repetition rate of 50 Hz. Each bunch is separated by 0.5ns, therefore, it

will be necessary to integrate over multiple bunch crossing when reading out the detectors. This places tight constraints on all detector electrical readout speeds and time resolutions.

Beam-Related Backgrounds at CLIC

The primary sources of background for the CLIC experiment are as follows:

- e^+e^- pair creation from the interaction of a beamstrahlung photons with the opposing beam. The different mechanisms for pair creation are as follows:
 - **Coherent pair production.** This mechanism involves the interaction of a real beamstrahlung photon with the electromagnetic field from the opposing beam.
 - **Trident pair production.** This mechanism involves the interaction of a virtual beamstrahlung photon with the electromagnetic field from the opposing beam.
 - **Incoherent pair production.** This mechanism involves the interaction of a real or virtual beamstrahlung photon with the individual particles in the opposing beam.
- $\gamma\gamma \rightarrow \text{Hadron}$ from the interaction of real or virtual beamstrahlung photons with each other. Example Feynman diagrams for such processes is shown in figure ??.
- Beam halo muons that arise from interactions of the beam particles during collimation. The dominant mechanisms producing beam halo muons are photon conversions into muon pairs ($\gamma e^- \rightarrow \mu^+ \mu^- e^-$) and annihilation of positrons with atomic e^- into muon pairs ($e^+ e^- \rightarrow \mu^+ \mu^-$) [12].

Each of these has to be properly addressed to get a true measure of the physics potential at CLIC. Coherent and trident pair production is not a dominant source of background as they are produced at low transverse momenta, as figure 1.1 shows, and a simple cut would veto these backgrounds. This is not the case for incoherent pair production of e^+e^- , which are dominant in the forward regions of the detector, and $\gamma\gamma \rightarrow \text{Hadron}$, which are dominant in the tracker and the calorimeters (with the exception of low radii in the calorimeter endcaps) [8, 13]. Beam halo muons are not a major source of background either as they can be easily removed during the

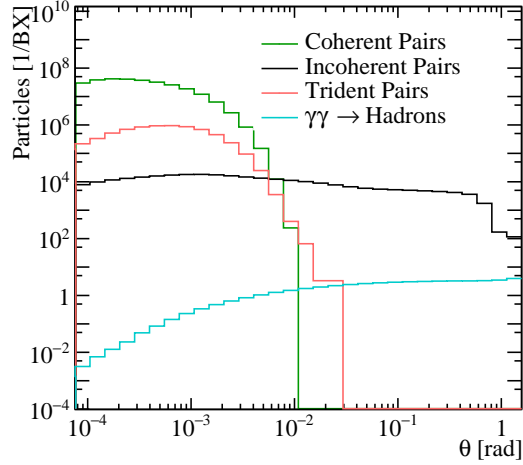


Figure 1.1: Angular distribution of number of particles for beam induced backgrounds for CLIC at $\sqrt{s} = 3$ TeV. Taken from CLIC CDR.

reconstruction due to the clear signal they create in the detector. An algorithm was developed within the PandoraPFA framework for this purpose and it was found to be highly effective at removing the beam halo muons background [8].

$\gamma\gamma \rightarrow$ Hadron events are the most dominant source of background to consider at CLIC as these events deposit more energy throughout the detector than incoherent pair production of e^+e^- events [8]. The effect of the $\gamma\gamma \rightarrow$ Hadron background is incorporated into this analysis by overlaying $\gamma\gamma \rightarrow$ Hadron events onto the event samples used in this analysis. The overlaid backgrounds are added prior to reconstruction so that their effect on the reconstruction is fully accounted for. For a given event the exact number of background events overlaid is drawn from a Poisson distribution with a mean of 3.2 (1.3) events per bunch crossing at 3 (1.4) TeV. While incoherent pairs are still a source of background they will produce a second order effect in comparison to the $\gamma\gamma \rightarrow$ Hadron events.

The PFO choices described in section 2.9 are applied to veto the effect of PFOs that arise from the overlaid $\gamma\gamma \rightarrow$ Hadron events.

Chapter 2.

The Sensitivity of CLIC to Anomalous Gauge Couplings through Vector Boson Scattering

“Kids, you tried your best, and you failed miserably. The lesson is, never try.”

— Homer Simpson

2.1. Motivation

Vector boson scattering is the interaction of the form $VV \rightarrow VV$ where V is any of the electroweak gauge bosons W^+ , W^- , Z or γ . This is an interesting process to look at because it gives a detailed understanding of how the Higgs of the standard model is able to unitarise the otherwise unbounded cross section for longitudinal gauge boson scattering. Vector boson scattering also provides insights into beyond standard model physics that impacts the electroweak sector through the probing of anomalous triple and quartic gauge couplings. Presented in this section is an analysis into the sensitivity of CLIC to two of these anomalous quartic gauge couplings through the vector boson scattering process.

Triple and quartic gauge couplings lead to interactions of the form $V \rightarrow VV$ and $VV \rightarrow VV$ respectively, where V is any of the electroweak gauge bosons W^+ ,

W^- , Z or γ . In the standard model there are five permissible vertices, shown in figure ??, which arise from the kinematic term in the standard model Lagrangian $\mathcal{L}_{kin} = -\frac{1}{4}B_{\mu\nu}B^{\mu\nu} - \frac{1}{4}W_{\mu\nu}W^{\mu\nu}$.

Anomalous triple and quartic gauge couplings are introduced as parameters in effective field theory models (EFTs). These anomalous couplings can either modify the standard model triple and quartic gauge boson couplings or introduce new triple and quartic couplings that were previously forbidden.

EFT models work under the assumption than new physics exists at an energy scale, Λ , which is assumed to be much higher than the energy scales currently accessible to modern day particle physics experiments. Furthermore, in limit $\Lambda \rightarrow \infty$ the standard model should be reproduced as the new physics becomes kinematically inaccessible. Such models are thus, by construction, guaranteed to recover the current best model of particle physics, while still introducing a regime for new physics. Such theories are model independent, giving them a wide span in the search for new physics.

A classic example of this is the Fermi theory for beta decay whereby the weak interaction occurring when a neutron decays into a proton, electron and anti-neutrino can be, at energies much below the mass of the mediating W boson, can be treated as a four-point vertex with quartic coupling strength G_F , the Fermi Coupling constant. (Feynamn Diagram if keep)

This analysis examines the anomalous quartic gauge couplings α_4 and α_5 , which are introduced as part of an EFT described in chapter THEORY CHAPTER. They appear in the Lagrangian through the following terms

$$\alpha_4[\text{Tr}(V^\mu V_\mu)]^2 \text{ and } \alpha_5 \text{Tr}(V^\mu V_\nu) \text{Tr}(V^\nu V_\mu) \quad (2.1)$$

Where V_μ corresponds, in the proper gauge, to a linear combination of the massive gauge bosons W^+ , W^- and Z . These terms effect the coupling constants for the standard model vertices $W^+W^- \rightarrow W^+W^-$ and $W^+W^- \rightarrow ZZ$ as well as introducing the new vertex $ZZ \rightarrow ZZ$.

Vector boson scattering is an appropriate process to consider for a sensitivity study into the anomalous gauge couplings α_4 and α_5 as quartic gauge boson self-interaction

vertices will be present in the dominant channels for such interactions (FEYNMAN DIAGRAM).

As CLIC is purposefully designed for high precision measurements it is ideal for a study into vector boson scattering. The application of Particle Flow Calorimetry with fine granularity calorimeters gives CLIC excellent jet energy resolution, which allows CLIC to clearly characterise the multi-jet final states that will be present in a study of vector boson scattering. When considering the invariant mass of these paired up jets, the nominal jet energy resolution for CLIC, allows for accurate separation of W and Z bosons, which will be invaluable in event selection. Such precision also helps CLIC to characterise final states containing missing energy in the form of neutrinos, which will also be present in a vector boson scattering study. The standard model cross sections for vector boson scattering final states at the proposed running energies for CLIC are such that there is a significant signal sample size for such an analysis. Finally, such a study at CLIC offers the potential to be several orders of magnitude more precise than the complementary studies at the LHC due to the reduction in hadronic backgrounds and the high \sqrt{s} for the interaction offered by colliding leptons instead of protons.

As the hadronic channels are the dominant decay modes of the W and the Z boson, with branching fractions of the order of 70% for both (REFERENCE PDG), and given CLIC has excellent jet energy resolution that analysis focuses solely upon the vector boson scattering processes where the outgoing bosons decay purely hadronically. The vector boson scattering dominated signal final states at CLIC that contain hadronic decay products for the bosons are thus: $\nu\nu\text{qqqq}$, $\text{l}\nu\text{qqqq}$ and llqqqq .

2.2. Event Generation, Simulation and Reconstruction

Check this doesn't sound too close to Higgs paper.

Events were generated for this analysis using the Whizard [7, 11] 1.95 program. Due to the presence of beamstrahlung photons in the CLIC beam events were generated from collisions of e^+e^- , $e^+\gamma$, γe^- and $\gamma\gamma$. The energy spectra used for all particles involved in these collisions accounted for the effects of radiation in the form of beamstrahlung photons and the intrinsic energy spread of the CLIC beam. Furthermore, events involving the interaction between the electromagnetic field of the beam particles involving quasi-real photon mediators with low momenta, described

by the Weizsäcker-Williams approximation or the Equivalent Photon Approximation (EPA), were generated using Whizard and included in this analysis. Fragmentation and hadronisation was implemented using Pythia 6.4 [14], which was tuned for OPAL e^+e^- collision data recorded at LEP (see [8] for details). The decays of tau leptons was simulated using Tauola [16]. The full list of events simulated for this analysis, along with their standard model cross section at 1.4 TeV can be found in table 2.1. The samples generated comprise all final states that would be relevant either as signal or background processes, for an analysis involving the purely hadronic decay channels involved in a vector boson scattering process. In full they are:

- Vector boson scattering signal final states that are expected to show sensitivity to the anomalous couplings: $e^+e^- \rightarrow \nu\nu qqqq$, $e^+e^- \rightarrow l\nu qqqq$ and $e^+e^- \rightarrow llqqqq$
- Four jet final states arising from e^+e^- interactions: $e^+e^- \rightarrow qqqq$.
- Two jet final states arising from e^+e^- interactions: $e^+e^- \rightarrow \nu\nu qq$, $e^+e^- \rightarrow l\nu qq$, $e^+e^- \rightarrow llqq$ and $e^+e^- \rightarrow qq$.
- Four jet final states arising from the interactions of either e^+ or e^- with a beamstrahlung photon: $\gamma_{BS} e^- \rightarrow qqqqe^-$, $e^+ \gamma_{BS} \rightarrow qqqqe^+$, $\gamma_{BS} e^- \rightarrow qqqq\nu$ and $e^+ \gamma_{BS} \rightarrow qqqq\nu$.
- Four jet final states arising from the interactions of either e^+ or e^- with the electromagnetic field of the opposing beam particle. These cross sections are calculated using the EPA approximation, which represents the electromagnetic field of the opposing beam particle as a series of photons and so the final states appear as interactions of e^+ or e^- with photons: $\gamma_{EPA} e^- \rightarrow qqqqe^-$, $e^+ \gamma_{EPA} \rightarrow qqqqe^+$, $\gamma_{EPA} e^- \rightarrow qqqq\nu$ and $e^+ \gamma_{EPA} \rightarrow qqqq\nu$.
- Four jet final states arising from the interaction of the electromagnetic fields of opposing beam particles using the EPA approximation: $\gamma_{EPA} \gamma_{EPA} \rightarrow qqqq$.
- Four jet final states arising from the interaction of the electromagnetic field of either e^+ or e^- using the EPA approximation with a beamstrahlung photon: $\gamma_{EPA} \gamma_{BS} \rightarrow qqqq$ or $\gamma_{BS} \gamma_{EPA} \rightarrow qqqq$.
- Four jet final states arising from the interaction of two beamstrahlung photons: $\gamma_{BS} \gamma_{BS} \rightarrow qqqq$.

Note: In the above list $q = u, d, s, c$ and $b, l = e, \mu, \tau$ and $\nu = \nu_e, \nu_\mu$ and ν_τ .

The samples used in this analysis were simulated with the CLIC_ILD detector model [1]. The simulation was performed in MOKKA [10], a GEANT4 [2] wrapper providing detailed geometric descriptions of detector concepts for the linear collider. Events were reconstructed using MARLIN [5], a c++ framework designed for reconstruction at the linear collider. PandoraPFA [9, 15] was used to apply Particle Flow Calorimetry in the reconstruction, the full details of which can be found in chapter PANDORA CHAPTER.

The CLIC_ILD is a variant of the ILD detector described in section REFERENCE. The only significant difference between the models is that CLIC_ILD has a 60 layer scintillator-tungsten HCal in comparison to the 48 layers found in the default ILD detector. The thicknesses of the layers in the HCal models are identical, so the extra layers correspond to an increase in the total thickness of the HCal. This is needed to compensate for the effects of leakage at the higher energies seen by the CLIC experiment in comparison to the ILC.

2.3. Modelling of Anomalous Gauge Couplings

It was necessary when generating samples that are sensitive to the anomalous gauge couplings α_4 and α_5 to use Whizard version 1.97, instead of the previously quoted version 1.95. This change was required as version 1.97 contained a unitarisation scheme that ensured cross sections for processes involving longitudinal gauge boson scattering were bound the energies considered i.e. the TeV scale.

The sensitivity of an individual event to the anomalous gauge couplings is determined through an event weight. This weight is given by the ratio of the squares of the matrix element used in the cross section calculation, one matrix element using non-zero values of α_4 and α_5 and the other matrix element using the standard model values of α_4 and α_5 , i.e. 0. The weight varies as a function of α_4 and α_5 as well as varying on an event by event basis as the kinematics of the final state changes. Examples of the event weights as a function of α_4 and α_5 for selected events is shown in figure 2.1 for 1.4 TeV $\nu\nu\text{qqqq}$ final state events.

This reweighting procedure has many advantages over the alternative of generating new samples with fixed α_4 and α_5 , notably the absence of systematic errors arising from new event generation, simulation and reconstruction. Only final states showing a

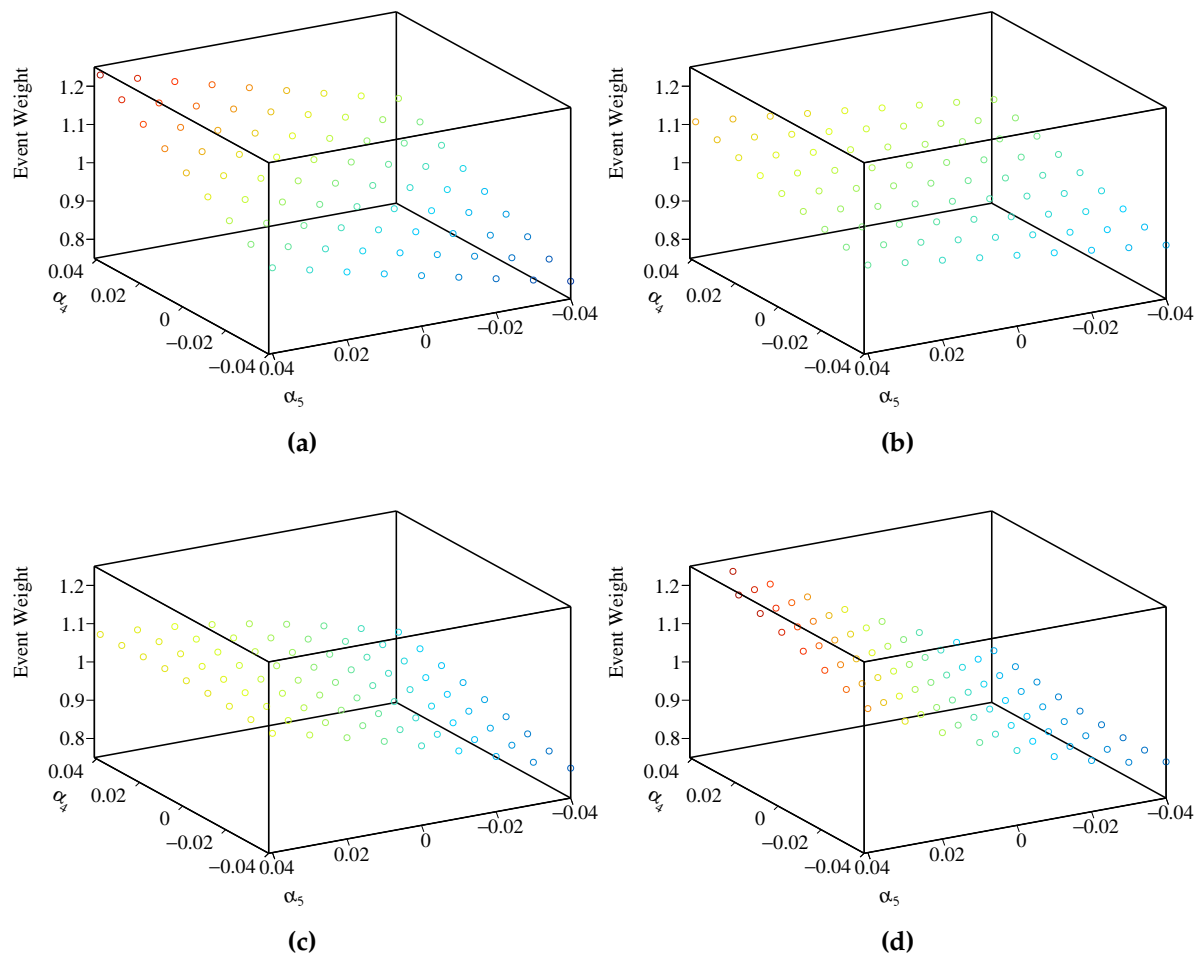


Figure 2.1.: A selection of plots showing how the event weight changes when varying the anomalous couplings α_4 and α_5 for 1.4TeV $\nu\nu\text{qqqq}$ final state events.

Final State	Cross Section 1.4 TeV [fb]
$e^+e^- \rightarrow \nu\nuqqqq$	24.7
$e^+e^- \rightarrow l\nuqqqq$	110.4
$e^+e^- \rightarrow llqqqq$	62.1
$e^+e^- \rightarrow qqqq$	1245.1
$e^+e^- \rightarrow \nu\nuqq$	787.7
$e^+e^- \rightarrow l\nu qq$	4309.7
$e^+e^- \rightarrow llqq$	2725.8
$e^+e^- \rightarrow qq$	4009.5
$\gamma_{\text{EPA}} e^- \rightarrow qqqqe^-$	287.1
$\gamma_{\text{BS}} e^- \rightarrow qqqqe^-$	1160.7
$e^+ \gamma_{\text{EPA}} \rightarrow qqqqe^+$	286.9
$e^+ \gamma_{\text{BS}} \rightarrow qqqqe^+$	1156.3
$\gamma_{\text{EPA}} e^- \rightarrow qqqq\nu$	32.6
$\gamma_{\text{BS}} e^- \rightarrow qqqq\nu$	136.9
$e^+ \gamma_{\text{EPA}} \rightarrow qqqq\nu$	32.6
$e^+ \gamma_{\text{BS}} \rightarrow qqqq\nu$	136.4
$\gamma_{\text{EPA}} \gamma_{\text{EPA}} \rightarrow qqqq$	753.0
$\gamma_{\text{EPA}} \gamma_{\text{BS}} \rightarrow qqqq$	4034.8
$\gamma_{\text{BS}} \gamma_{\text{EPA}} \rightarrow qqqq$	4018.7
$\gamma_{\text{BS}} \gamma_{\text{BS}} \rightarrow qqqq$	21406.2

Table 2.1.: Cross sections of signal and background processes at 1.4 TeV. In the above table $q \in u, \bar{u}, d, \bar{d}, s, \bar{s}, c, \bar{c}, b$ or \bar{b} while $l \in e^\pm, \mu^\pm$ or τ^\pm and $\nu \in \nu_e, \nu_\mu$ and ν_τ . The subscript EPA or BS for the incoming photons indicate whether the photon is generated from the equivalent photon approximation or beamstrahlung.

sensitivity to α_4 and α_5 require reweighting and to determine those states a comparison was made between the cross section using the standard model values of α_4 and α_5 , i.e. 0, and the same calculation using non-zero values of these couplings at 1.4 TeV. This comparison was performed on all of the generated samples listed in table 2.1 and the results for samples showing sensitivity to the couplings can be found in table 2.2

The cross sections were found to differ when using non-zero values for the anomalous couplings in comparison to the standard model prediction only for the vector boson scattering signal final states $\nu\nuqqqq$, $l\nuqqqq$ and $llqqqq$. In reality, non-zero anomalous couplings would change the cross sections of all processes considered,

however, the sensitivity would only arise from high order terms in the Lagrangian. Such terms would not be dominant in determining the cross section and so are omitted from the generator making certain final states appear invariant to changes in the anomalous couplings.

Final State	Cross Section [fb] ($\alpha_4 = \alpha_5 = 0.00$)	Cross Section [fb] ($\alpha_4 = \alpha_5 = 0.05$)	Percentage Change[%]	CLIC Cross Section [fb]
$e^+ e^- \rightarrow \nu\nu qqqq$	20.8	34.6	+66.3	24.7
$e^+ e^- \rightarrow l\nu qqqq$	112	113	+0.9	115.3
$e^+ e^- \rightarrow llqqqq$	59.7	68.6	+14.9	62.1

Table 2.2.: Cross section for selected processes for given value of α_4 and α_5 at 1.4 TeV.

The cross section calculations show that the most sensitive final state to the anomalous gauge couplings is $\nu\nu qqqq$, therefore, this analysis will focus entirely upon this final state. Furthermore, as the $l\nu qqqq$ final state has a much reduced sensitivity in comparison to the $\nu\nu qqqq$ state and as the $llqqqq$ can be easily vetoed from the analysis, as will be shown in subsequent chapters, it is only necessary to consider the sensitivity of the $\nu\nu qqqq$ final state. For the aforementioned reasons the $l\nu qqqq$ and $llqqqq$ final states will be treated as backgrounds that are invariant to changes in the anomalous couplings α_4 and α_5 .

In order to determine the anomalous gauge coupling sensitive event weights it was necessary to use the anomalous gauge coupling model in Whizard, which enforces a unit CKM matrix. In the context of vector boson scattering and the $\nu\nu qqqq$ final state, which is the only final state requiring reweighting, this restricts the decays of the W^- boson to $d\bar{u}$ and $s\bar{c}$, the W^+ boson to $u\bar{d}$ and $c\bar{s}$ and the Z boson to $u\bar{u}$, $d\bar{d}$, $s\bar{s}$, $c\bar{c}$ and $b\bar{b}$. In comparison, the non-unit CKM matrix allows for extra decay modes, however, this was found to have a negligible effect on the samples when comparing several reconstructed level distributions. Furthermore, flavour tagging of jets was not used in this analysis as it offered negligible gains when performing event selection and so any bias in quark flavour present due to the enforcement of a unit CKM in the signal samples did not impact this analysis.

2.4. Data Analysis

The focus of this section is to describe the post reconstruction procedure applied to the signal and background events, described in ??, to extract the relevant information needed for this sensitivity study.

2.4.1. Jet Finding

After the reconstruction two further processors are applied to remove reconstructed particle flow objects (PFOs) that originate from beam related backgrounds, described in section CLIC BEAM CHAPER, from the event. The first processor is the CLICTrackSelection, designed to veto poorly reconstructed tracks and to reject tracks where the time of arrival at the calorimeter between the helix fit to the track and to a straight line of flight differ by 50ns. The latter would indicate the tracked particle does not create the calorimetric energy deposits that it has been associated to. The second processor is the CLICPfoSelector, which applies cuts to the p_T and timing information of the PFOs. These cuts vary as a function of position in the detector and the reconstructed particle type in an attempt to target the regions of the detector where background, primarily low $p_T \gamma\gamma \rightarrow \text{Hadrons}$ events, are more prominent. Three configurations of the CLICPfoSelector have been developed for the CLIC environment and were considered for this analysis. They are, in order of increasing background rejection, the Loose, Default and Tight selections. The full details of each can be found here [9].

After the application of the CLICTrackSelection and CLICPfoSelector the MarlinFastJet processor, a wrapper for the FastJet [4] processor, was used to cluster the events into four jets. These jets are then paired up to form two candidate bosons. This pairing is performed on the assumption that the correct pairing is achieved when the difference between the invariant masses of the jet pairs is a minimum. In the case of the signal final state, $\nu\nu qqqq$, it is assumed that the four jets have arisen from the hadronic decays of the outgoing bosons involved in the vector scattering process and that the pairing of the jets gives candidate bosons that match the outgoing bosons involved in vector boson scattering.

The jet clustering was done using the longitudinally invariant k_t jet algorithm in exclusive mode. In contrast to the inclusive mode, the exclusive mode allows the user

to request a fixed number of jets in the output from MarlinFastJet. The longitudinally invariant k_t algorithm proceeds as follows:

- For each pair of particles, i and j, the k_t distance, d_{ij} , and beam distance, $d_{iB} = p_t^2$, are calculated.

$$d_{ij} = \min(p_{ti}^2, p_{tj}^2) \Delta R_{ij}^2 / R^2 \quad (2.2)$$

where $\Delta R_{ij}^2 = (y_i - y_j)^2 + (\phi_i - \phi_j)^2$, p_t is the transverse momentum of the particle with respect to the beam axis, y_i is the rapidity of particle i and ϕ_i is the azimuthal angle of particle i. R is a configurable parameter that typically is of the order of 1.

- The minimum distance, d_{\min} , of all the k_t and beam distances is found. If the minimum occurs for a k_t distance, merge particles i and j, summing their 4-momenta in the energy combination scheme. If the beam distance is the minimum, declare particle i to be apart of the "beam" jet. Remove this particle from the list of particles and do not included in the final jet output.
- Repeat until the requested number of jets have been created, or inclusive mode no particles are left in the event.

Two other clustering algorithms were considered, but, as figure 2.11 shows, were found to be inappropriate for the experimental conditions at CLIC. These alternative algorithm choices are applied in the same manor as the longitudinally invariant k_t algorithm, however, they differ in their for the k_t distance, d_{ij} , and beam distance, d_{iB} .

The first alternative jet algorithm considered was the k_t algorithm for e^+e^- colliders (or Durham algorithm) where $d_{ij} = 2\min(E_i^2, E_j^2)(1 - \cos\theta_{ij})$ and d_{iB} is not used. θ_{ij} is the opening angle of particles i and j meaning that in the collinear limit d_{ij} corresponds to the relative transverse momenta of the particles. The major failure of this algorithm when applied to CLIC is the absence of d_{iB} , which leads to many beam related background particles being associated to jets. As figure 2.11 shows, the invariant mass of the paired jets, which is expected to be centred around the W and Z boson masses, is much larger than expected, due to the presence of the beam related backgrounds in the jets. Also this algorithm is not invariant to boosts along the beam direction making it inappropriate to use at CLIC as the beam induced backgrounds modify the nominal collision kinematics.

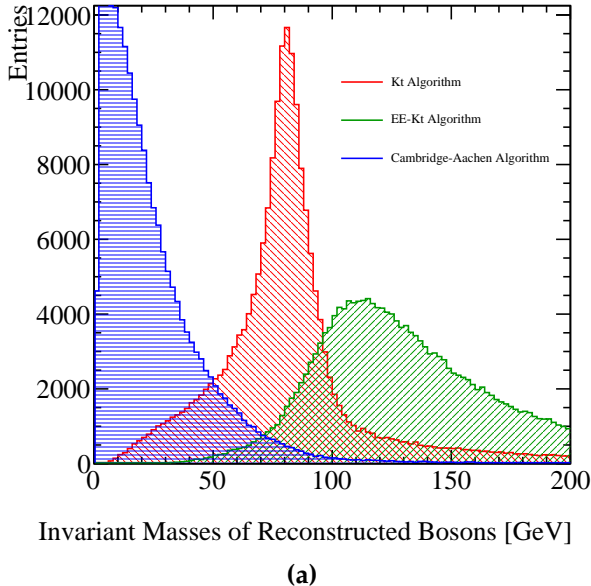


Figure 2.2.: Reconstructed masses for different choices of jet algorithm for 1.4 TeV $\nu\nu\text{qqqq}$ events. These masses arise by forcing the reconstructed events into 4 jets and then pairing up the jets into pairs such that the reconstructed invariant masses of the pairs are closest to each other. These samples should be dominated by vector boson scattering involving pairs of W bosons and so it is expected that a peak at the W boson true mass should be observed. As this does not occur for the Cambridge-Aachen algorithm or the ee_kt algorithm they were deemed unsuitable for this analysis at both 1.4. In the case of the kt algorithm and the ee_kt algorithm an R parameter of 0.7 was used.

The second alternative jet algorithm considered was the Cambridge/Aachen jet algorithm where $d_{ij} = \Delta R_{ij}^2 / R^2$ and $d_{iB} = 1$. This algorithm gave poor performance as it does not account for the transverse momentum or energy of the particles being clustered. In essence, this is a cone clustering algorithm with a cone radius defined through $\Delta R_{ij} = R$, which even for large R was found to discard too much energy in the event to be useful for this analysis. This can be seen in figure 2.11 as the invariant mass of the paired jets is much lower than expected. This algorithm is useful for events with highly boosted jets, but at CLIC the jets are too disperse for this algorithm to be successfully applied.

Optimal Jet Finding Algorithm

Optimisation of the jet algorithm configuration was performed on the choice of PFO selection as well as the value of the R parameter used in the longitudinally invariant

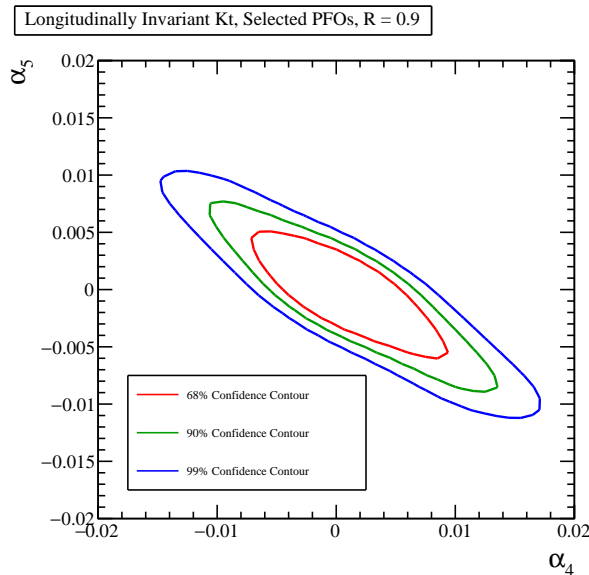
k_t algorithm. The optimal configuration for the jet algorithm at 1.4 TeV was found to use default selected PFOs and an R parameter of 0.9.

The procedure involved performing the sensitivity study, described in section BLAH??, using solely the $\nu\nu\text{qqqq}$ signal final state. This procedure leads to the construction of a χ^2 surface from which confidence contours can be extracted in the α_4 and α_5 space. The χ^2 surface for the optimal jet configuration at 1.4 TeV using the $\nu\nu\text{qqqq}$ signal final state is shown in figure 2.3a. This procedure ensured that the optimisation was done with respect to the physics of interest without having to perform the jet reconstruction procedure for the large number of background events.

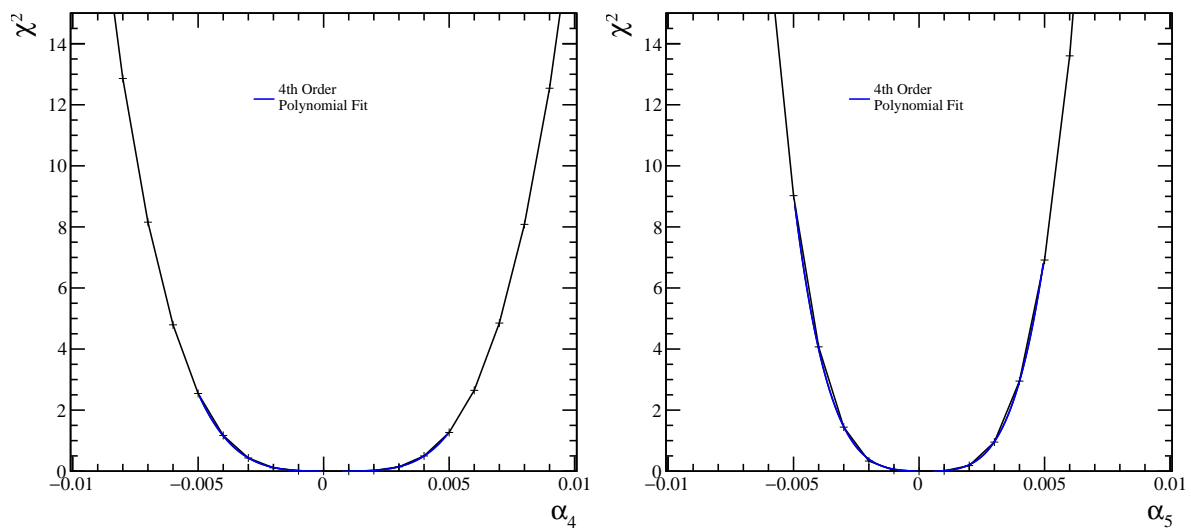
Confidence limits on the individual parameters α_4 and α_5 were determined by setting the corresponding coupling term to zero and examining the now one dimensional χ^2 distribution. A fourth order polynomial was fitted to the minima of this distribution and the one sigma confidence limit defined using $\Delta\chi^2$ of 1. $\Delta\chi^2$ is defined as the change in χ^2 with respect to the minima in the χ^2 surface. Note that for the two dimensional χ^2 surface a one sigma confidence limit is given by a $\Delta\chi^2$ of 2.28 due to the additional degree of freedom in the fit. The one dimensional χ^2 distribution for α_4 and α_5 , assuming $\alpha_5 = 0$ and $\alpha_4 = 0$ respectively, for the optimal jet configuration at 1.4 TeV using the $\nu\nu\text{qqqq}$ signal final state is shown in figures 2.3b and 2.3c. Using these distributions the one sigma confidence limits on α_4 is -0.0038 to 0.0047 and on α_5 is -0.0027 to 0.0030.

2.4.2. Lepton Finding

An isolated lepton finder was included in the analysis chain in an attempt to reject background events containing leptons. The isolated lepton finder attempts to find whether a PFO is an electron or muon based on the calorimetric energy deposits before then placing cuts on the tracks associated to the PFOs to determine whether the tracks originate from the impact point. Finally isolation cuts restricting the energy in a cone surrounding the PFO are applied to ensure the particles does not belong to a jet. The efficiency of the lepton finder is summarised in table 2.3.



(a) χ^2 sensitivity contours in α_4 and α_5 space.



(b) χ^2 as a function of α_4 assuming $\alpha_5 = 0$.

(c) χ^2 as a function of α_5 assuming $\alpha_4 = 0$.

Figure 2.3.: χ^2 sensitivity distributions for the qqqqvv final state arising from a fit to $\cos\theta_{\text{jets}}^*$ at 1.4 TeV for the optimal jet reconstruction parameters.

Final State	$\epsilon_{\text{Lepton Finding}}$
$e^+ e^- \rightarrow \nu\nu qqqq$	99.7
$e^+ e^- \rightarrow l\nu qqqq$	48.9

Table 2.3.: The efficiency of isolated lepton finding at 1.4 TeV for the $\nu\nu qqqq$ and $l\nu qqqq$ final states. Efficiency here is defined as the fraction of events where no isolated leptons were found.

2.4.3. Discriminant Variables

The next stage of the analysis involved the calculation of a number of event-based variables that were found to be useful for this analysis. The variables can be divided into four categories:

- **Particle level** variables:
 - Number of PFOs.
 - Particle type and energy of the highest energy PFO.
 - Energy of the highest energy electron.
 - Cosine of the polar angle of the highest energy track.
- **Candidate boson** variables:
 - Energy of candidate bosons.
 - Invariant mass of the bosons.
 - Acolinearity of the boson pair, which is defined as 180 degrees minus the opening angle of the pair of bosons in the rest frame of the detector.
 - Acolinearities of the pair of jets forming each the two candidate boson.
 - $\text{Cos}(\theta_{Bosons}^*)$. Cosine of the opening of the bosons in the rest frame of the boson pair.
 - $\text{Cos}(\theta_{Jets}^*)$. Cosine of the opening of the jets forming each candidate in the rest frame of the candidate boson.
- **Event based** variables:
 - The invariant mass of the visible system.

- The vector sum of the transverse momentum of all PFOs in the event.
- The cosine of the polar angle of the missing 3-momentum assuming a collision at the nominal centre of mass energy.
- Principle thrust T , defined through the following equation

$$T = \max_{\bar{\mathbf{n}}} \left(\frac{\sum_i \mathbf{p}_i \cdot \bar{\mathbf{n}}}{\sum_i |\mathbf{p}_i|^2} \right) \quad (2.3)$$

Where p_i are the components of the momenta of PFO i in the rest frame of the detector, $\bar{\mathbf{n}}$ is unit vector and the sum Σ_i runs over all particles in the event.

- Sphericity, defined through the sphericity tensor S^{ab} :

$$S^{ab} = \frac{\sum_i p_i^\alpha p_j^\alpha}{\sum_{i,\alpha=1,2,3} |p_i^\alpha|^2} \quad (2.4)$$

Where p_i are the components of the momenta of PFO i in the rest frame of the detector and the sum Σ_i runs over all particles in the event. Sphericity is defined as $S = \frac{3}{2}(\lambda_2 + \lambda_3)$, where λ_i are the eigenvalues of the sphericity tensor defined such $\lambda_1 \geq \lambda_2 \geq \lambda_3$. This provides a measure of how spherical the reconstructed event topology is with isotropic events having $S \approx 1$, while two jet events have $S \approx 0$.

- Aplanarity defined as $\frac{3}{2}\lambda_3$ where λ_3 is an eigenvalue of the sphericity tensor. This provides a measure of whether an event is linear or planar in shape.

- Jet clustering parameters y_{ij} .

2.5. Event Selection

As discussed earlier the signal events for this analysis contain the $\nu\nu\text{qqqq}$ final state. The processes to be considered in this analysis alongside the signal are events that would topologically look similar to signal in the detector. This includes events that could be confused with 4 jet events with missing energy, while excluding those events with large numbers of high energy leptons that could be vetoed easily during the analysis stage. In full the list includes:

Final State	Cross Section 1.4 TeV [fb]
$e^+e^- \rightarrow \nu\nu qqqq$	24.7
$e^+e^- \rightarrow l\nu qqqq$	110.4
$e^+e^- \rightarrow llqqqq$	62.1
$e^+e^- \rightarrow qqqq$	1245.1
$e^+e^- \rightarrow \nu\nu qq$	787.7
$e^+e^- \rightarrow l\nu qq$	4309.7
$e^+e^- \rightarrow llqq$	2725.8
$e^+e^- \rightarrow qq$	4009.5
$\gamma_{\text{EPA}} e^- \rightarrow qqqqe^-$	287.1
$\gamma_{\text{BS}} e^- \rightarrow qqqqe^-$	1160.7
$e^+ \gamma_{\text{EPA}} \rightarrow qqqqe^+$	286.9
$e^+ \gamma_{\text{BS}} \rightarrow qqqqe^+$	1156.3
$\gamma_{\text{EPA}} e^- \rightarrow qqqq\nu$	32.6
$\gamma_{\text{BS}} e^- \rightarrow qqqq\nu$	136.9
$e^+ \gamma_{\text{EPA}} \rightarrow qqqq\nu$	32.6
$e^+ \gamma_{\text{BS}} \rightarrow qqqq\nu$	136.4
$\gamma_{\text{EPA}} \gamma_{\text{EPA}} \rightarrow qqqq$	753.0
$\gamma_{\text{EPA}} \gamma_{\text{BS}} \rightarrow qqqq$	4034.8
$\gamma_{\text{BS}} \gamma_{\text{EPA}} \rightarrow qqqq$	4018.7
$\gamma_{\text{BS}} \gamma_{\text{BS}} \rightarrow qqqq$	21406.2

Table 2.4.: Cross sections of signal and background processes at 1.4 TeV. In the above table $q \in u, \bar{u}, d, \bar{d}, s, \bar{s}, c, \bar{c}, b$ or \bar{b} while $l \in e^\pm, \mu^\pm$ or τ^\pm and $\nu \in \nu_e, \nu_\mu$ and ν_τ . The subscript EPA or BS for the incoming photons indicate whether the photon is generated from the equivalent photon approximation or beamstrahlung.

Equivalent Photon Approximation (EPA) processes model the electromagnetic field of a charged particle as virtual photons. BS (beamstrahlung) processes involve photons that have been radiated from incoming charged particles due to interactions with the electromagnetic field of the opposite beam. The energy spectrum of the incoming particles for CLIC at the relevant operating energy is used to model the energy of these incoming photons. Included in this study are photon-photon interactions from photons appearing from the EPA and beamstrahlung processes.

2.5.1. Pre Selection

The primary selection of the $\nu\nu\text{qqqq}$ signal will be done using a multivariate analysis, however, in an attempt to veto trivial backgrounds a simple cut based preselection is applied. Cuts are applied to the transverse momentum, invariant mass of the visible system and the number of isolated leptons. The raw distributions of these variables is shown in figure 2.4. Based on these distributions the following cuts were applied:

- Transverse momentum > 100 GeV. This cut is effective due to the presence of missing energy in the form of neutrinos in the signal final state.
- Visible mass of the system > 200 GeV. This cut is effective for accounting for the missing energy of the neutrinos in the final state along the longitudinal direction of the detector instead.
- Number of isolated leptons = 0. This cut vetoes a large number of events with leptons in the final state. The effect of these preselection cuts can be found in table 1.3. While a large fraction of the signal events are lost through these cuts, particularly the transverse momentum cuts, a much large fraction of background events are removed justifying the cut.

The event numbers for the signal and background are shown in table 2.5 as these cuts are cumulatively applied. These numbers are normalised to the correct luminosity for CLIC running at 1.4 TeV. As is expected the large transverse momentum cut removes practically all backgrounds containing no missing energy. The invariant mass cut removes significant fractions of two quark and missing energy events. Finally, the isolated lepton finder cut removes backgrounds containing visible leptonic final states.

2.5.2. MVA

A multivariate analysis was applied to the data set to refine the selection using the TMVA toolkit [6]. The following variables were used for training the TMVA selection.

- Number of PFOs in the event.
- Highest energy PFO type.
- Transverse momentum of the event.

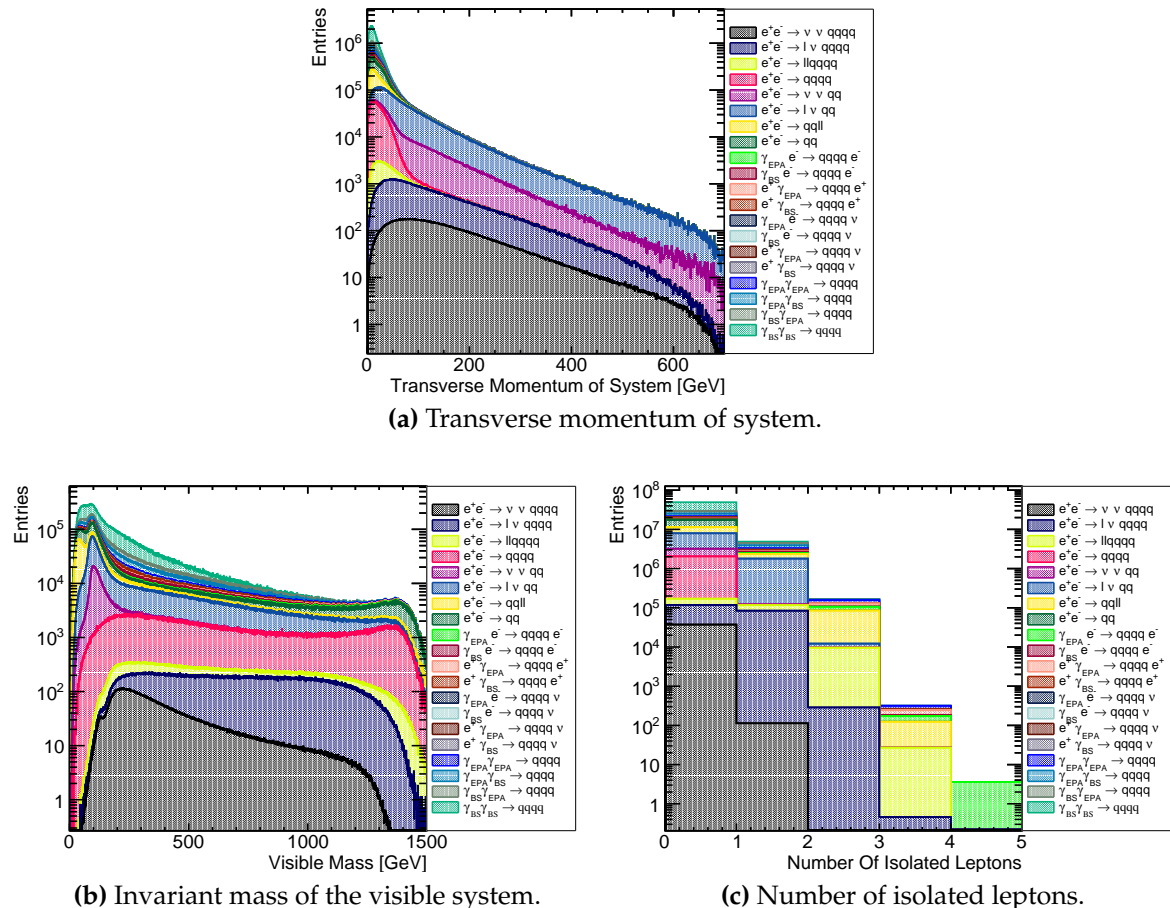


Figure 2.4.: Distribution of variables cut on in the preselection at 1.4 TeV.

Final State	Raw Event Numbers	$p_T > 100 \text{ GeV}$	$p_T > 100 \text{ GeV} \&$ $M_{\text{Vis}} > 200 \text{ GeV}$	$p_T > 100 \text{ GeV} \&$ $M_{\text{Vis}} > 200 \text{ GeV} \&$ $N_{\text{Isolated Leptons}} = 0$
$e^+ e^- \rightarrow \nu\nu qqqq$	37,050	23,800	21,080	21,020
$e^+ e^- \rightarrow l\nu qqqq$	165,600	81,620	80,840	42,410
$e^+ e^- \rightarrow llqqqq$	93,150	1,151	1,140	700
$e^+ e^- \rightarrow qqqq$	1,868,000	6,487	6,467	6,445
$e^+ e^- \rightarrow \nu\nu qq$	1,181,000	514,100	50,260	50,150
$e^+ e^- \rightarrow l\nu qq$	6,464,000	2,003,000	1,259,000	567,600
$e^+ e^- \rightarrow llqq$	4,088,000	7,754	7,351	5,643
$e^+ e^- \rightarrow qq$	6,011,000	34,610	34,130	34,070
$\gamma_{\text{EPA}} e^- \rightarrow qqqqe^-$	430,600	2,463	2,446	865
$\gamma_{\text{BS}} e^- \rightarrow qqqqe^-$	1,306,000	1,382	1,340	1,002
$e^+ \gamma_{\text{EPA}} \rightarrow qqqqe^+$	430,300	2,846	2,823	1,121
$e^+ \gamma_{\text{BS}} \rightarrow qqqqe^+$	1,301,000	654	643	469
$\gamma_{\text{EPA}} e^- \rightarrow qqqq\nu$	48,890	17,450	13,490	8,852
$\gamma_{\text{BS}} e^- \rightarrow qqqq\nu$	154,000	56,380	36,350	35,900
$e^+ \gamma_{\text{EPA}} \rightarrow qqqq\nu$	48,890	17,520	13,550	8,928
$e^+ \gamma_{\text{BS}} \rightarrow qqqq\nu$	153,400	56,280	36,340	35,900
$\gamma_{\text{EPA}} \gamma_{\text{EPA}} \rightarrow qqqq$	1,129,000	3,160	3,079	1,563
$\gamma_{\text{EPA}} \gamma_{\text{BS}} \rightarrow qqqq$	4,539,000	5,325	5,270	3,987
$\gamma_{\text{BS}} \gamma_{\text{EPA}} \rightarrow qqqq$	4,521,000	3,810	3,730	2,318
$\gamma_{\text{BS}} \gamma_{\text{BS}} \rightarrow qqqq$	20,550,000	2,445	2,445	1,673

Table 2.5.: Number of events passing the various cuts applied in the preselection at 1.4 TeV.

Event numbers are normalised to the correct luminosity for CLIC at 1.4 TeV. p_T is the transverse momentum of the event, M_{Vis} is the visible mass and $N_{\text{Isolated Leptons}}$ is the number of isolated leptons in the event. In the above table $q \in u, \bar{u}, d, \bar{d}, s, \bar{s}, c, \bar{c}, b$ or \bar{b} while $l \in e^\pm, \mu^\pm$ or τ^\pm and $\nu \in \nu_e, \nu_\mu$ and ν_τ . The subscript EPA or BS for the incoming photons indicate whether the photon is generated from the equivalent photon approximation or beamstrahlung.

- $\cos\theta_{\text{Missing}}$. The cosine of the polar angle of the missing momentum.
- $\cos\theta_{\text{Highest Energy Track}}$. The cosine of the polar angle of the track with the largest momentum.
- y_i, y_{i+1} . Jet clustering parameters ranging from $i = 0$ to 6.

- Principle thrust, sphericity and aplanarity as defined in section BLAH.
- Energy of the highest energy electron in the event.
- Energy of the highest energy PFO in the event.
- Energy of the reconstructed bosons.
- Acolinearity of the reconstructed boson pair.
- Invariant mass of the reconstructed bosons.
- Acolinearity of the jets forming the reconstructed bosons.

It was found that the best MVA algorithm for both performance and speed was the booted decision tree (BDT) when comparing different methods using the default settings. Add plot here.

The BDT was further optimised by varying the number of trees used, the depth of the trees and the number of cuts applied. The results shown in the rest of this section use the optimal configuration. For the optimal BDT configuration a significance of $S/\sqrt{(S+B)} = 53.6$ was obtained.

The event numbers passing the BDT cut can be found in table 2.6. The performance of the BDT is shown in figure 2.5, which shows the change in the distribution of the invariant mass of the reconstructed bosons as the MVA is applied. As expected the dominant background processes after the MVA is applied are those that will look identical to the visible signal process i.e. $qqqq$ and missing energy. Two smaller sources of background that pass the MVA exists, those where two jets and missing energy are confused as four jets and missing energy and those where a lepton is not properly reconstructed and the events look like four jets and missing energy.

The summary of the selection procedure is given in table 2.7.

2.6. Effect of Anomalous Coupling/Fitting Methodology

The metric used to determine the optimal jet algorithm for this analysis is the sensitivity of the pure signal final state, $\nu\nu qqqq$, to the anomalous gauge couplings. Pure signal was used in the optimisation to avoid the need to process the large number of

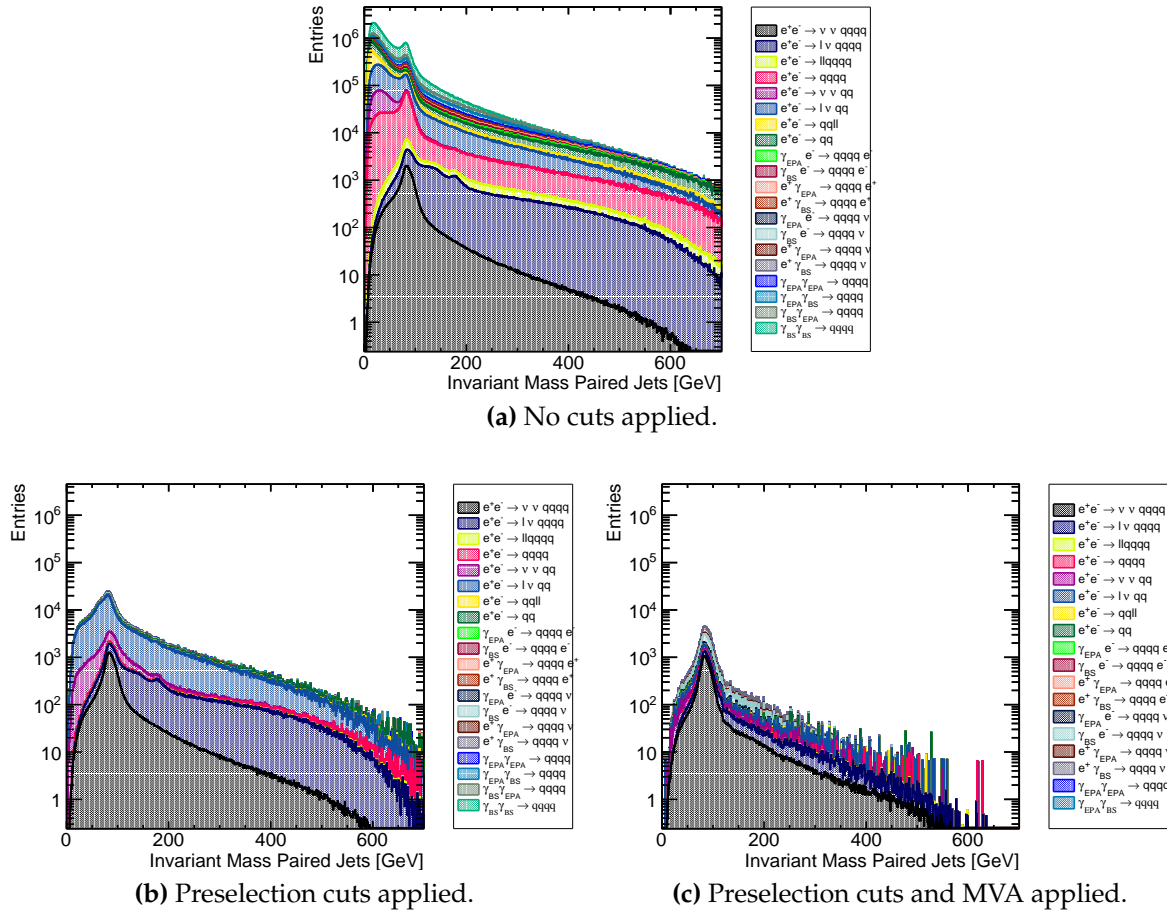


Figure 2.5.: Impact of preselection and MVA on the reconstructed invariant mass of the bosons arising from jet pairing at 1.4 TeV.

Final State	Raw Event Numbers	Post MVA Selection Numbers
$e^+e^- \rightarrow \nu\nuqqqq$	37,050	14,770
$e^+e^- \rightarrow l\nuqqqq$	165,600	6,159
$e^+e^- \rightarrow llqqqq$	93,150	80
$e^+e^- \rightarrow qqqq$	1,868,000	1,264
$e^+e^- \rightarrow \nu\nuqq$	1,181,000	3,286
$e^+e^- \rightarrow l\nu qq$	6,464,000	6,262
$e^+e^- \rightarrow llqq$	4,088,000	234
$e^+e^- \rightarrow qq$	6,011,000	1,016
$\gamma_{\text{EPA}} e^- \rightarrow qqqqe^-$	430,300	20
$\gamma_{\text{BS}} e^- \rightarrow qqqqe^-$	1,306,000	42
$e^+ \gamma_{\text{EPA}} \rightarrow qqqqe^+$	430,300	19
$e^+ \gamma_{\text{BS}} \rightarrow qqqqe^+$	1,301,000	44
$\gamma_{\text{EPA}} e^- \rightarrow qqqq\nu$	48,890	3,552
$\gamma_{\text{BS}} e^- \rightarrow qqqq\nu$	154,000	18,540
$e^+ \gamma_{\text{EPA}} \rightarrow qqqq\nu$	48,890	3,652
$e^+ \gamma_{\text{BS}} \rightarrow qqqq\nu$	153,400	18,770
$\gamma_{\text{EPA}} \gamma_{\text{EPA}} \rightarrow qqqq$	1,129,000	68
$\gamma_{\text{EPA}} \gamma_{\text{BS}} \rightarrow qqqq$	4,539,000	55
$\gamma_{\text{BS}} \gamma_{\text{EPA}} \rightarrow qqqq$	4,521,000	0
$\gamma_{\text{BS}} \gamma_{\text{BS}} \rightarrow qqqq$	20,550,000	0

Table 2.6.: Number of events passing the MVA selection at 1.4 TeV. Event numbers are normalised to the correct luminosity for CLIC at 1.4 TeV. The subscript EPA or BS for the incoming photons indicate whether the photon is generated from the equivalent photon approximation or beamstrahlung.

background files for each iteration of the jet algorithm considered, while still basing the optimisation on the physics of interest. The focus of this section in the description of the fitting technique that will be used for both jet algorithm optimisation and in the final sensitivity study.

2.6.1. Choice of Fitting Distribution

The sensitivity of CLIC to the anomalous gauge couplings is determined through the use of a χ^2 fit to the distribution of $\cos\theta_{jets}^*$. For a given event, the jet clustering and

Final State	ϵ_{presel}	ϵ_{BDT}	N_{BDT}
$e^+ e^- \rightarrow \nu\nu qqqq$	56.7%	39.9%	14,770
$e^+ e^- \rightarrow l\nu qqqq$	25.7%	3.7%	6,159
$e^+ e^- \rightarrow \nu\nu qq$	4.3%	0.3%	3,286
$e^+ e^- \rightarrow l\nu qq$	8.8%	0.1%	6,262
$\gamma_{\text{EPA}} e^- \rightarrow qqqq\nu$	18.0%	7.3%	3,552
$\gamma_{\text{BS}} e^- \rightarrow qqqq\nu$	23.2%	12.0%	18,540
$e^+ \gamma_{\text{EPA}} \rightarrow qqqq\nu$	18.2%	7.5%	3,652
$e^+ \gamma_{\text{BS}} \rightarrow qqqq\nu$	23.4%	12.2%	18,770

Table 2.7.: Selection summary at 1.4TeV. The subscript EPA or BS for the incoming photons indicate whether the photon is generated from the equivalent photon approximation or beamstrahlung. Channels omitted from this table have less than 1,500 events in the post MVA selection.

pairing proceeds as described in section ?? and leads to the event being clustered into four jets, which are then paired up to give two candidate bosons. θ_{jets}^* is defined as the opening angle of the jets in the rest frame of these candidate bosons. The distribution of $\cos\theta_{\text{jets}}^*$ proved to be highly sensitive to the anomalous gauge couplings as shown in figure 2.6.

The distribution of $\cos\theta_{\text{Bosons}}^*$ was also considered for this sensitivity study, however, it proved to be less sensitive than $\cos\theta_{\text{jets}}^*$. This can be seen when comparing figures 2.6 and 2.7. θ_{Bosons}^* is defined as the opening angle between the two candidate bosons two bosons in the rest frame of the candidate boson pair. Furthermore, it was found that the χ^2 distribution formed from the two dimensional distribution of $\cos\theta_{\text{jets}}^*$ against $\cos\theta_{\text{Bosons}}^*$ did not significantly benefit the sensitivity in comparison using the one dimensional distribution of $\cos\theta_{\text{jets}}^*$ and therefore was not considered for this analysis.

2.6.2. Application Of Anomalous Gauge Coupling Event Weights

As described in section ??, event weights are used to determine the sensitivity of CLIC to the anomalous gauge couplings. These event weights are extracted on an event by event basis for the signal final state $\nu\nu qqqq$ from the generator software Whizard. To achieve a smooth χ^2 distribution a fine sampling of the $\cos\theta_{\text{jets}}^*$ distribution in the α_4 and α_5 space is needed. However, as extracting the event weights is highly CPU

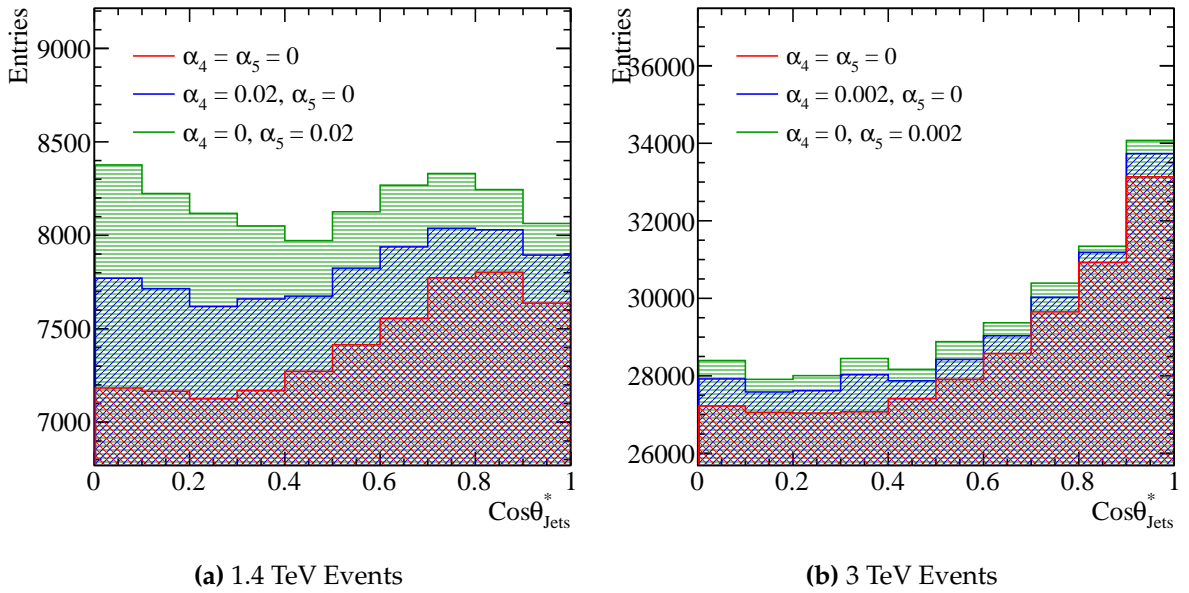


Figure 2.6.: Sensitivity of $\cos\theta_{\text{jets}}^*$ to anomalous couplings at 1.4 and 3 TeV. The jet algorithm used for this example was the longitudinally invariant kt algorithm with an R parameter of 0.7. This sample corresponds to pure signal of hadronic decays in vector boson scattering i.e. $\nu\nu\text{qqqq}$.

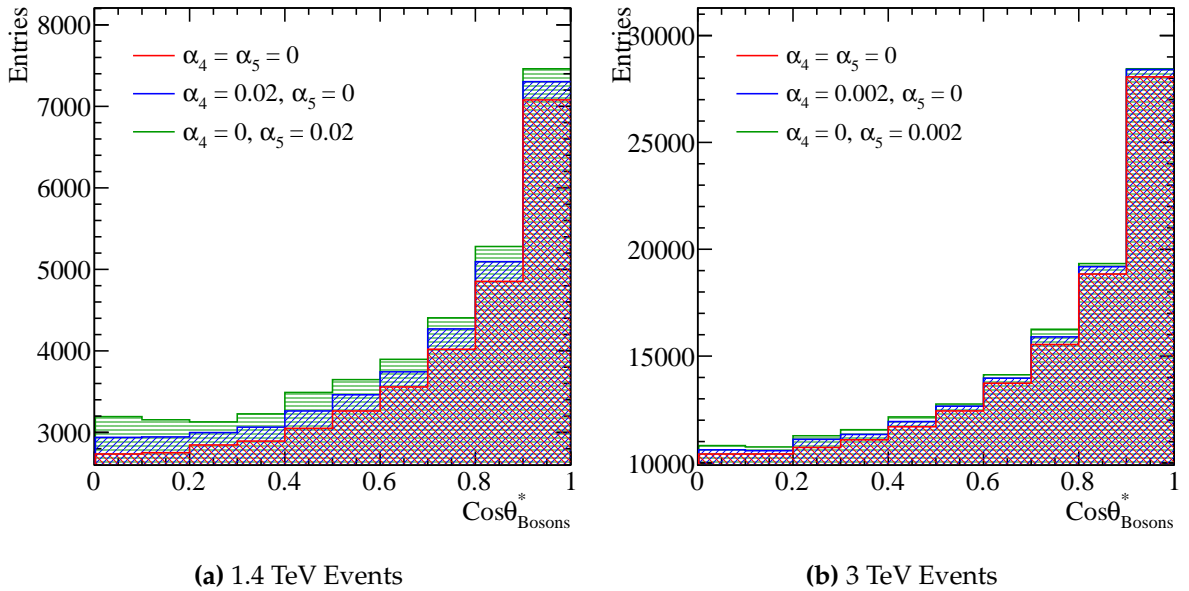


Figure 2.7.: Sensitivity of $\cos\theta_{\text{Bosons}}^*$ to anomalous couplings at 1.4 and 3 TeV. The jet algorithm used for this example was the longitudinally invariant kt algorithm with an R parameter of 0.7. This sample corresponds to pure signal of hadronic decays in vector boson scattering i.e. $\nu\nu\text{qqqq}$.

intensive, it is unfeasible to produce a finely sampled grid of event weights on an event by event basis by calling the generator. To resolve this issue, an interpolation scheme was applied to determine the event weights within a sampled region of the α_4 and α_5 space. This allows for an infinite sampling of the $\cos\theta_{Jets}^*$ distribution in the space of α_4 and α_5 within the sampled region, without having to call the generator an infinite number of times.

A bicubic interpolation scheme, cubic interpolation along two dimensions, was applied to the event weights that were extracted from the generator. This procedure is best illustrated by showing the interpolated surface superimposed with the raw event weights from the generator, which is shown for several $\nu\nu\text{qqqq}$ events at 1.4 TeV in figure 2.8 (ADD 3 TEV). This interpolation scheme produces a smooth and continuous surface that is sufficiently accurate for the fitting procedure applied in this analysis.

For reference at 1.4 TeV event weights were produced from the generator, Whizard, by stepping along α_4 and α_5 in steps of 0.01 ranging from -0.07 to 0.07, as shown in figure 2.1, while at 3 TeV event weights were samples in steps of 0.00025 from -0.0045 to 0.0045. These ranges proved to be sufficient for the contours of interest for the CLIC sensitivity analysis at these energies.

2.6.3. Determination of Sensitivity

The sensitivity of CLIC to the anomalous gauge couplings α_4 and α_5 was determined using a χ^2 of the following form:

$$\chi^2 = \sum_i \frac{(O_i - E_i)^2}{E_i} \quad (2.5)$$

Here, where O_i is the observed, or data, bin content for bin i in the distribution of $\cos\theta_{Jets}^*$ produced with event weights corresponding to zero α_4 and α_5 and E_i is the expected, or Monte-Carlo, bin content for bin i produced with event weights corresponding to non-zero α_4 and α_5 . The distribution of $\cos\theta_{Jets}^*$ was binned in a histograms containing 10 bins ranging from 0 to 1, as shown in figure 2.6. This binning was selected to maximise the sensitivity of the distribution, while minimising the

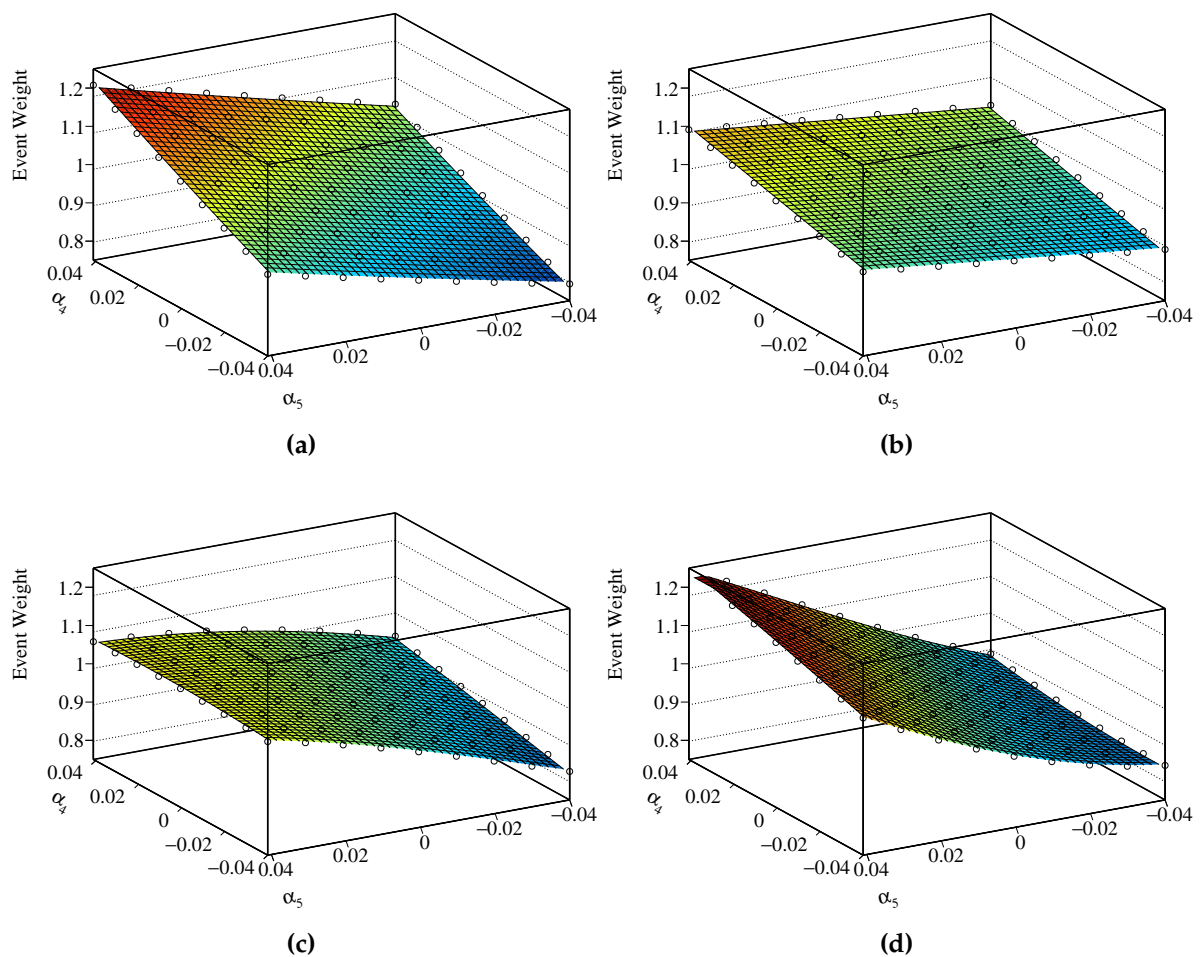


Figure 2.8: A selection of plots showing how the event weight changes when varying the anomalous couplings α_4 and α_5 for 1.4TeV $\nu\nu qqqq$ final state events. The hollow circles show the event weight produced from the generator while the surface shown is found using bicubic interpolation between those points.

effect of large bin by bin fluctuations arising from individual events with large event weights.

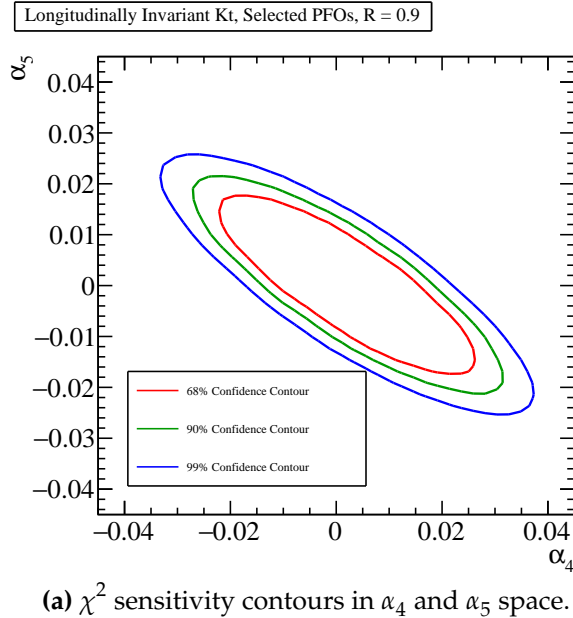
Confidence limits that describe the sensitivity of CLIC to the anomalous gauge couplings, were found by examining the χ^2 surface in α_4 and α_5 space. Deviations about the minima of this surface, which by construction occurs at $\alpha_4 = \alpha_5 = 0$, yield confidence limits that indicate the probability of observing a particular value of α_4 and α_5 based on the $\cos\theta_{jets}^*$ distribution. The confidence limits used in subsequent sections, 68%, 90% and 99%, are defined using fixed deviations from the minima of χ^2 contours of 2.28, 4.61 and 9.21 respectively. These numbers arise from the integral of the two dimensional χ^2 function.

It proved useful to consider the sensitivities to the individual parameters α_4 and α_5 independently. This was done by projecting out the $\alpha_4 = 0$ or $\alpha_5 = 0$ one dimensional χ^2 distribution from the two dimensional χ^2 previously discussed. It was then possible to extract the sensitivity to an individual parameters using confidence limits arising from the integral of the one dimensional χ^2 function i.e. 68% confidence limit occurs for $\chi^2 = 0.989$. In subsequent chapters these are the sensitivities quoted for individual anomalous gauge coupling parameters.

HERE

2.7. Results

The sensitivity of the CLIC experiment to the anomalous gauge couplings α_4 and α_5 at 1.4 TeV is shown in figure 2.9a. This result shows the sensitivity after the application of preselection and MVA described in sections 2.5.1 and 2.5.2 purposed to remove the included background channels, described in section 2.2. These contours yield the one σ confidence limit on the measurement of α_4 to the range -0.00831, 0.0130 and similarly for the measurement of α_5 the range is -0.00606, 0.00904.



(a) χ^2 sensitivity contours in α_4 and α_5 space.

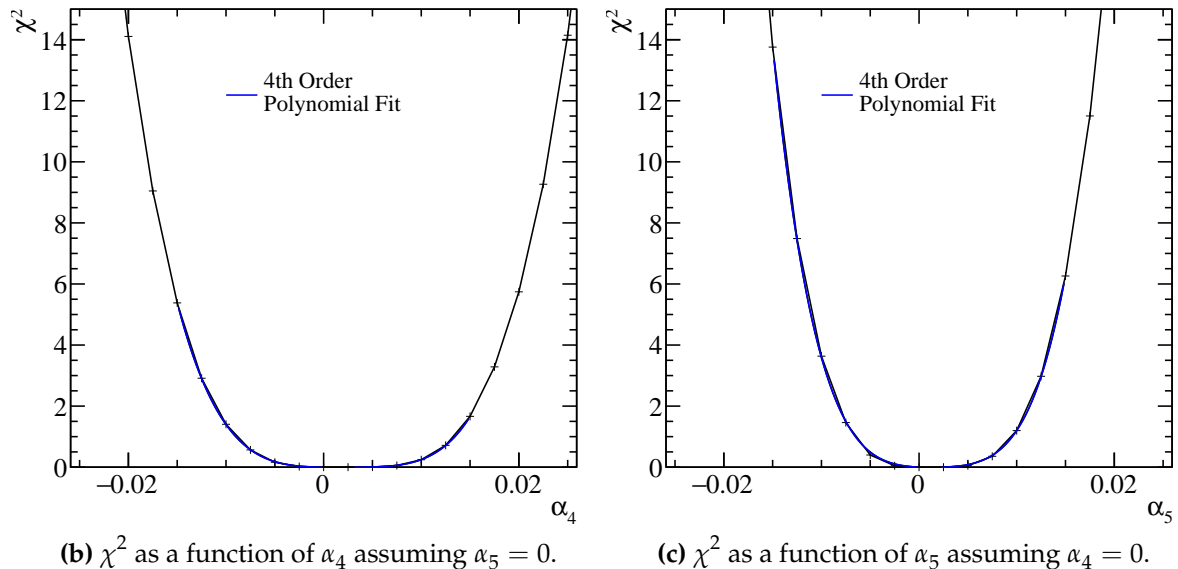


Figure 2.9.: χ^2 sensitivity distributions at 1.4 TeV arising from a fit to $\cos\theta_{\text{jets}}^*$. Results include the effect of backgrounds after the application of preselection and MVA.

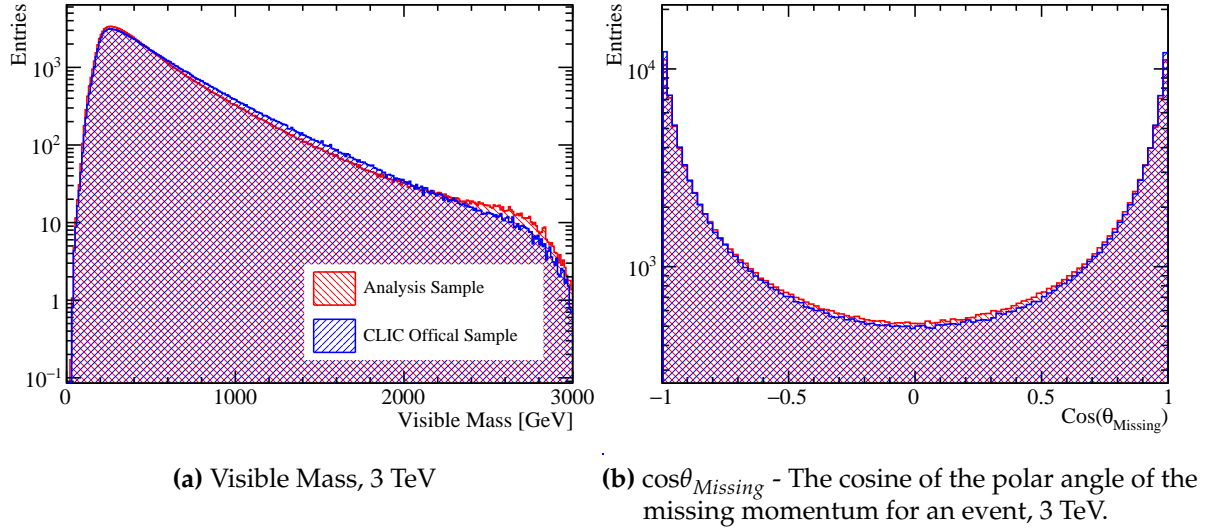


Figure 2.10.: Comparison of various distributions between samples used in this analysis and the official CLIC samples for the $\nu\nu\text{qqqq}$ final state at 3 TeV. Both samples have been normalised to the correct luminosity for CLIC running at 3 TeV.

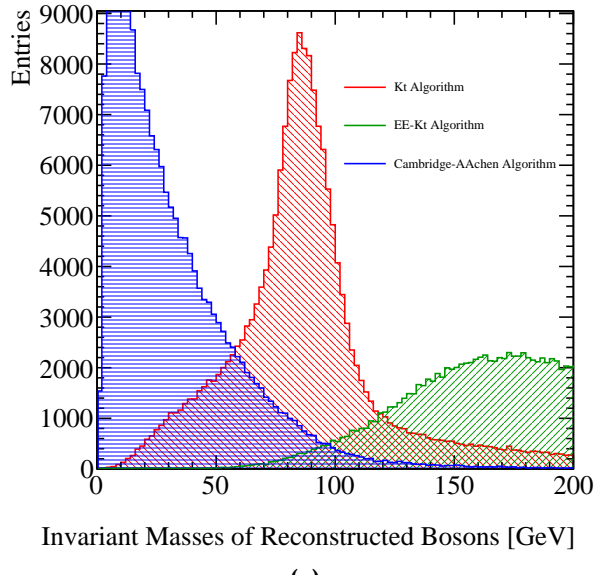


Figure 2.11.: Reconstructed masses for different choices of jet algorithm for 3 TeV $\nu\nu\text{qqqq}$ events. These masses arise by forcing the reconstructed events into 4 jets and then pairing up the jets into pairs such that the reconstructed invariant masses of the pairs are closest to each other. These samples should be dominated by vector boson scattering involving pairs of W bosons and so it is expected that a peak at the W boson true mass should be observed. As this does not occur for the Cambridge-Aachen algorithm or the ee_kt algorithm they were deemed unsuitable for this analysis at both 3 TeV. In the case of the kt algorithm and the ee_kt algorithm an R parameter of 0.7 was used.

Final State	Cross Section 1.4 TeV [fb]	Cross Section 3 TeV [fb]
$e^+ e^- \rightarrow \nu\nu qqqq$	24.7	71.5
$e^+ e^- \rightarrow l\nu qqqq$	110.4	106.6
$e^+ e^- \rightarrow llqqqq$	62.1	169.3
$e^+ e^- \rightarrow qqqq$	1245.1	546.5
$e^+ e^- \rightarrow \nu\nu qq$	787.7	1317.5
$e^+ e^- \rightarrow l\nu qq$	4309.7	5560.9
$e^+ e^- \rightarrow llqq$	2725.8	3319.6
$e^+ e^- \rightarrow qq$	4009.5	2948.9
$\gamma_{\text{EPA}} e^- \rightarrow qqqqe^-$	287.1	287.8
$\gamma_{\text{BS}} e^- \rightarrow qqqqe^-$	1160.7	1268.6
$e^+ \gamma_{\text{EPA}} \rightarrow qqqqe^+$	286.9	287.8
$e^+ \gamma_{\text{BS}} \rightarrow qqqqe^+$	1156.3	1267.3
$\gamma_{\text{EPA}} e^- \rightarrow qqqq\nu$	32.6	54.2
$\gamma_{\text{BS}} e^- \rightarrow qqqq\nu$	136.9	262.5
$e^+ \gamma_{\text{EPA}} \rightarrow qqqq\nu$	32.6	54.2
$e^+ \gamma_{\text{BS}} \rightarrow qqqq\nu$	136.4	262.3
$\gamma_{\text{EPA}} \gamma_{\text{EPA}} \rightarrow qqqq$	753.0	402.7
$\gamma_{\text{EPA}} \gamma_{\text{BS}} \rightarrow qqqq$	4034.8	2423.1
$\gamma_{\text{BS}} \gamma_{\text{EPA}} \rightarrow qqqq$	4018.7	2420.6
$\gamma_{\text{BS}} \gamma_{\text{BS}} \rightarrow qqqq$	21406.2	13050.3

Table 2.8.: Cross sections of signal and background processes at 1.4 and 3 TeV. In the above table $q \in u, \bar{u}, d, \bar{d}, s, \bar{s}, c, \bar{c}, b$ or \bar{b} while $l \in e^\pm, \mu^\pm$ or τ^\pm and $\nu \in \nu_e, \nu_\mu$ and ν_τ . The subscript EPA or BS for the incoming photons indicate whether the photon is generated from the equivalent photon approximation or beamstrahlung.

Final State	Cross Section [fb] ($\alpha_4 = \alpha_5 = 0.000$)	Cross Section [fb] ($\alpha_4 = \alpha_5 = 0.005$)	Percentage Change[%]	CLIC Cross Section [fb]
$e^+ e^- \rightarrow \nu\nu qqqq$	51.2	77.7	+51.8	71.5
$e^+ e^- \rightarrow l\nu qqqq$	111.9	115.9	+3.6	106.6
$e^+ e^- \rightarrow llqqqq$	169.7	161.7	-4.9	169.3

Table 2.9.: Cross section for selected processes for given value of α_4 and α_5 at 3 TeV.

2.8. Sensitivity at 3 TeV

2.8.1. Pre Selection - 3 TeV

Final State	Raw Event Numbers	$p_T > 100 \text{ GeV}$	$p_T > 100 \text{ GeV} \& M_{\text{Vis}} > 200 \text{ GeV}$	$p_T > 100 \text{ GeV} \& M_{\text{Vis}} > 200 \text{ GeV} \& N_{\text{Isolated Leptons}} = 0$
$e^+ e^- \rightarrow \nu\nu qqqq$	143,000	106,600	99,390	99,130
$e^+ e^- \rightarrow l\nu qqqq$	213,200	129,800	127,300	82,880
$e^+ e^- \rightarrow llqqqq$	338,600	32,750	31,010	23,550
$e^+ e^- \rightarrow qqqq$	1,093,000	40,180	37,360	37,300
$e^+ e^- \rightarrow \nu\nu qq$	2,634,000	1,333,000	380,100	379,500
$e^+ e^- \rightarrow l\nu qq$	11,120,000	4,240,000	2,479,000	1,836,000
$e^+ e^- \rightarrow llqq$	6,639,000	131,400	84,980	54,780
$e^+ e^- \rightarrow qq$	5,897,000	79,440	66,790	66,730
$\gamma_{\text{EPA}} e^- \rightarrow qqqqe^-$	575,600	57,920	54,640	34,480
$\gamma_{\text{BS}} e^- \rightarrow qqqqe^-$	2,004,000	99,930	90,750	83,440
$e^+ \gamma_{\text{EPA}} \rightarrow qqqqe^+$	575,600	57,990	54,290	34,190
$e^+ \gamma_{\text{BS}} \rightarrow qqqqe^+$	2,002,000	100,300	90,830	83,960
$\gamma_{\text{EPA}} e^- \rightarrow qqqq\nu$	108,400	63,780	60,660	46,380
$\gamma_{\text{BS}} e^- \rightarrow qqqq\nu$	414,700	233,800	215,600	213,600
$e^+ \gamma_{\text{EPA}} \rightarrow qqqq\nu$	108,400	64,230	61,130	46,720
$e^+ \gamma_{\text{BS}} \rightarrow qqqq\nu$	414,400	236,400	219,000	217,000
$\gamma_{\text{EPA}} \gamma_{\text{EPA}} \rightarrow qqqq$	805,400	54,010	48,720	37,730
$\gamma_{\text{EPA}} \gamma_{\text{BS}} \rightarrow qqqq$	3,828,000	150,800	131,600	114,500
$\gamma_{\text{BS}} \gamma_{\text{EPA}} \rightarrow qqqq$	3,825,000	150,600	133,600	116,900
$\gamma_{\text{BS}} \gamma_{\text{BS}} \rightarrow qqqq$	18,010,000	123,500	115,400	105,000

Table 2.10.: Number of events passing the various cuts applied in the preselection at 3 TeV. Event numbers are normalised to the correct luminosity for CLIC at 3 TeV. p_T is the transverse momentum of the event, M_{Vis} is the visible mass and $N_{\text{Isolated Leptons}}$ is the number of isolated leptons in the event. In the above table $q \in u, \bar{u}, d, \bar{d}, s, \bar{s}, c, \bar{c}, b$ or \bar{b} while $l \in e^\pm, \mu^\pm$ or τ^\pm and $\nu \in \nu_e, \nu_\mu$ and ν_τ . The subscript EPA or BS for the incoming photons indicate whether the photon is generated from the equivalent photon approximation or beamstrahlung.

The Sensitivity of CLIC to Anomalous Gauge Couplings through Vector Boson Scattering

36

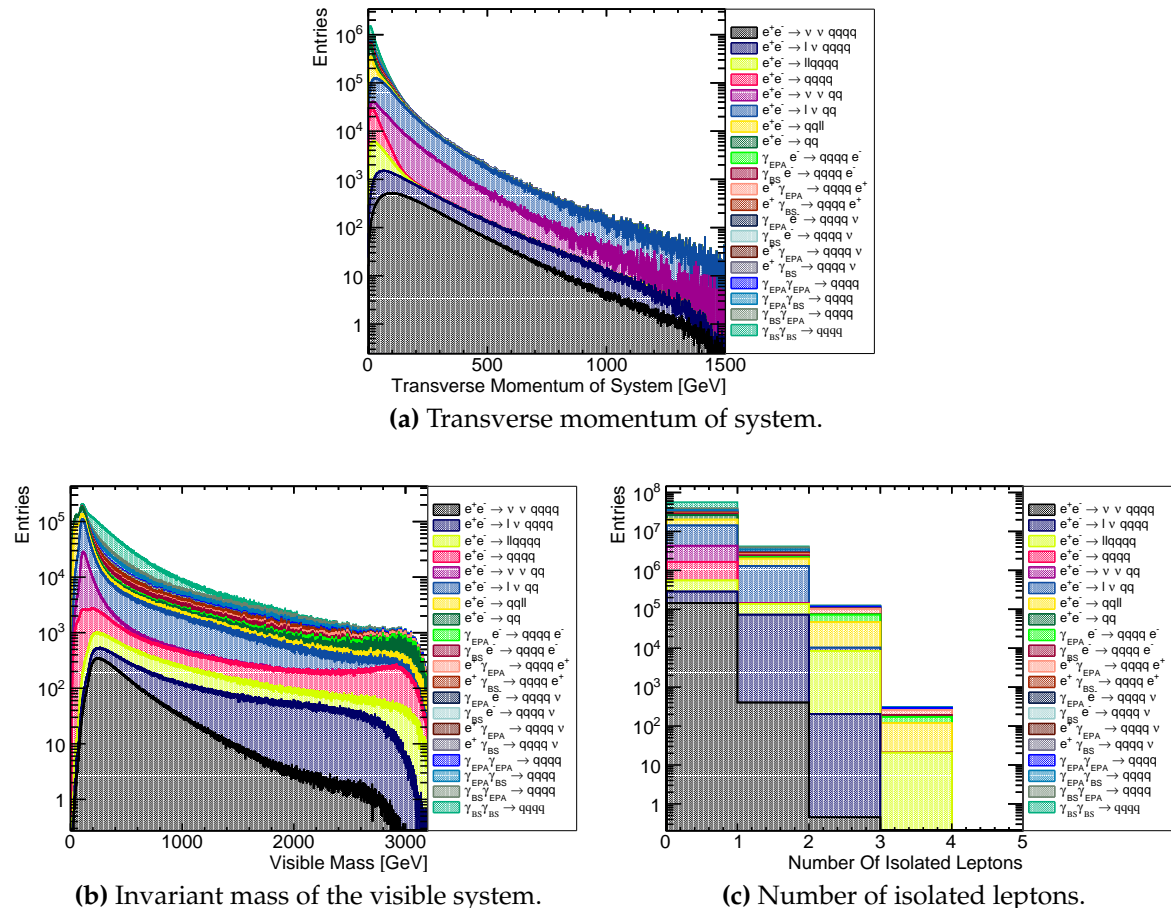


Figure 2.12.: Distribution of variables cut on in the preselection at 3 TeV.

2.8.2. MVA - 3 TeV

Final State	Raw Event Numbers	Post MVA Selection Numbers
$e^+e^- \rightarrow \nu\nu qqqq$	143,000	64,750
$e^+e^- \rightarrow l\nu qqqq$	213,200	23,310
$e^+e^- \rightarrow llqqqq$	338,600	2,409
$e^+e^- \rightarrow qqqq$	1,093,000	3,069
$e^+e^- \rightarrow \nu\nu qq$	2,634,000	19,040
$e^+e^- \rightarrow l\nu qq$	11,120,000	27,910
$e^+e^- \rightarrow llqq$	6,639,000	786
$e^+e^- \rightarrow qq$	5,897,000	1,335
$\gamma_{\text{EPA}} e^- \rightarrow qqqqe^-$	575,600	2,860
$\gamma_{\text{BS}} e^- \rightarrow qqqqe^-$	2,004,000	8,352
$e^+ \gamma_{\text{EPA}} \rightarrow qqqqe^+$	575,600	3,063
$e^+ \gamma_{\text{BS}} \rightarrow qqqqe^+$	2,002,000	8,090
$\gamma_{\text{EPA}} e^- \rightarrow qqqq\nu$	108,400	17,950
$\gamma_{\text{BS}} e^- \rightarrow qqqq\nu$	414,700	108,000
$e^+ \gamma_{\text{EPA}} \rightarrow qqqq\nu$	108,400	17,980
$e^+ \gamma_{\text{BS}} \rightarrow qqqq\nu$	414,400	109,700
$\gamma_{\text{EPA}} \gamma_{\text{EPA}} \rightarrow qqqq$	805,400	3,058
$\gamma_{\text{EPA}} \gamma_{\text{BS}} \rightarrow qqqq$	3,828,000	9,812
$\gamma_{\text{BS}} \gamma_{\text{EPA}} \rightarrow qqqq$	3,825,000	8,880
$\gamma_{\text{BS}} \gamma_{\text{BS}} \rightarrow qqqq$	18,010,000	2,213

Table 2.11.: Number of events passing the MVA selection at 3 TeV. Event numbers are normalised to the correct luminosity for CLIC at 3 TeV. The subscript EPA or BS for the incoming photons indicate whether the photon is generated from the equivalent photon approximation or beamstrahlung.

2.9. Optimisation of Jet Reconstruction

The jet algorithm used in this analysis is the longitudinally invariant kt algorithm as described in section 2.4.1. The parameters considered in this optimisation were the R parameter, used in the kt algorithm definition, and the PFO selection.

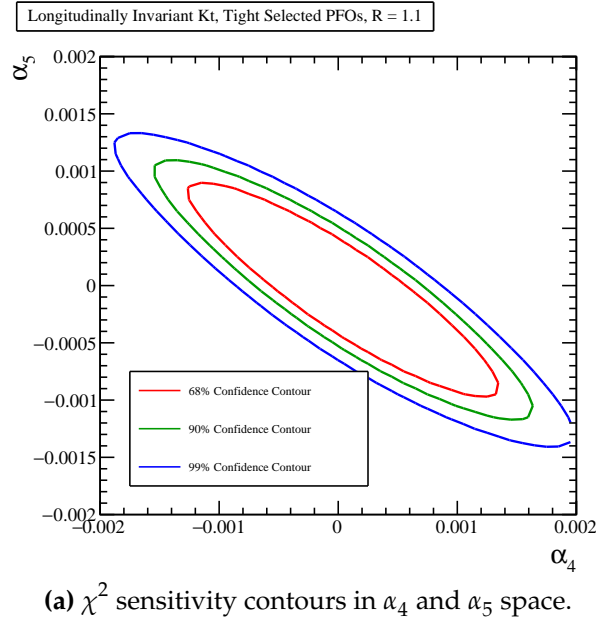
Final State	ϵ_{presel}	ϵ_{BDT}	N_{BDT}
$e^+e^- \rightarrow \nu\nu qqqq$	69.4%	45.3%	64,750
$e^+e^- \rightarrow l\nu qqqq$	38.9%	10.9%	23,310
$e^+e^- \rightarrow \nu\nu qq$	14.4%	0.7%	19,040
$e^+e^- \rightarrow l\nu qq$	16.5%	0.3%	27,910
$\gamma_{\text{BS}} e^- \rightarrow qqqqe^-$	4.1%	0.4%	8,352
$e^+ \gamma_{\text{BS}} \rightarrow qqqqe^+$	4.2%	0.4%	8,090
$\gamma_{\text{EPA}} e^- \rightarrow qqqq\nu$	42.8%	16.6%	17,950
$\gamma_{\text{BS}} e^- \rightarrow qqqq\nu$	51.6%	26.0%	108,000
$e^+ \gamma_{\text{EPA}} \rightarrow qqqq\nu$	43.1%	16.6%	17,980
$e^+ \gamma_{\text{BS}} \rightarrow qqqq\nu$	52.3%	26.5%	109,700
$\gamma_{\text{EPA}} \gamma_{\text{BS}} \rightarrow qqqq$	3.0%	0.3%	9,812
$\gamma_{\text{BS}} \gamma_{\text{EPA}} \rightarrow qqqq$	3.1%	0.2%	8,880

Table 2.12.: Selection summary at 3 TeV. The subscript EPA or BS for the incoming photons indicate whether the photon is generated from the equivalent photon approximation or beamstrahlung. Channels omitted from this table have less than 6,000 events in the post MVA selection.

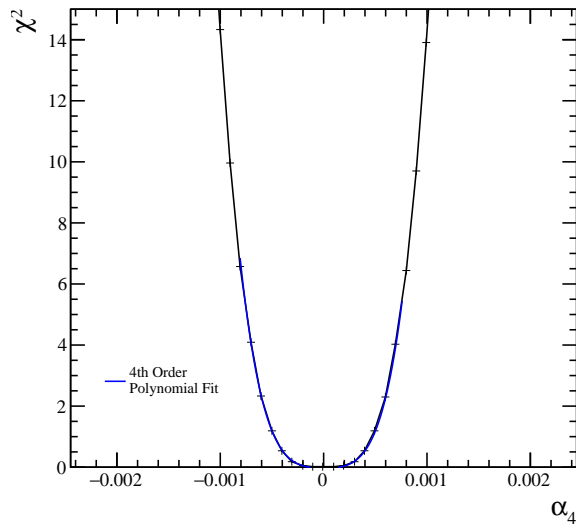
2.9.1. 3 TeV Optimal Jet Reconstruction

At 3 TeV the optimal sensitivity for the reconstructions considered is achieved for tight selected PFOs with an R parameter of 1.1 as can be seen from tables 2.13 and 2.14. The optimal contours can be found in figure 2.13a and the optimal 1D plot used to produce the errors references in the tables 2.13 and 2.14 can be found in figures 2.13b and 2.13c respectively. All other contours and plots for this optimisation can be found in the appendices.

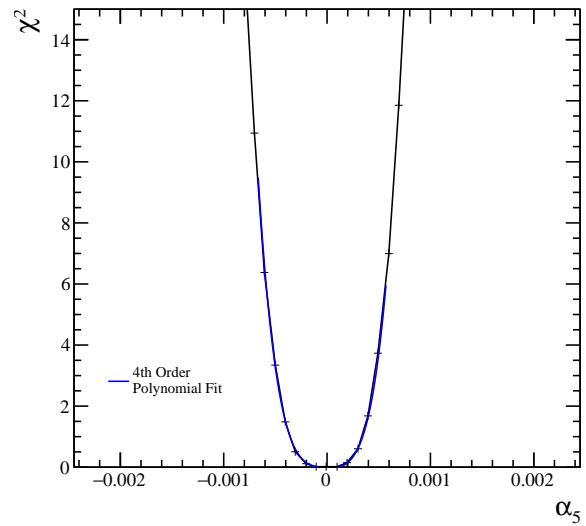
The gains in optimising the jet algorithm at 3 TeV are larger than those found at 1.4 TeV. The preference for the tight selected PFOs is to be expected as this configuration minimises the effect of beam induced backgrounds, which are more prominent at higher energies.



(a) χ^2 sensitivity contours in α_4 and α_5 space.



(b) χ^2 as a function of α_4 assuming $\alpha_5 = 0$.



(c) χ^2 as a function of α_5 assuming $\alpha_4 = 0$.

Figure 2.13.: χ^2 sensitivity distributions for the $qqqq\nu\nu$ final state arising from a fit to $\cos\theta_{\text{jets}}^*$ at 3 TeV for the optimal jet reconstruction parameters.

PFO Selection	Tight Selected PFOs	Selected PFOs	Loose Selected PFOs
R Parameter			
0.7	$-0.000530 + 0.000525$	$-0.000502 + 0.000507$	$-0.000547 + 0.000555$
0.9	$-0.000566 + 0.000555$	$-0.000539 + 0.000520$	$-0.000568 + 0.000553$
1.1	$-0.000472 + 0.000472$	$-0.000508 + 0.000492$	$-0.000504 + 0.000490$

Table 2.13.: Precision on measurement of α_4 at 3 TeV for different jet reconstruction parameters considering pure signal and applying a χ^2 fit to $\cos\theta_{Jets}^*$.

PFO Selection	Tight Selected PFOs	Selected PFOs	Loose Selected PFOs
R Parameter			
0.7	$-0.000393 + 0.000370$	$-0.000356 + 0.000348$	$-0.000357 + 0.000348$
0.9	$-0.000394 + 0.000365$	$-0.000392 + 0.000361$	$-0.000396 + 0.000368$
1.1	$-0.000351 + 0.000337$	$-0.000374 + 0.000354$	$-0.000353 + 0.000336$

Table 2.14.: Precision on measurement of α_5 at 3 TeV for different jet reconstruction parameters considering pure signal and applying a χ^2 fit to $\cos\theta_{Jets}^*$.

Appendix A.

Pointless extras

*“Le savant n’étudie pas la nature parce que cela est utile;
il l’étudie parce qu’il y prend plaisir,
et il y prend plaisir parce qu’elle est belle.”*

— Henri Poincaré, 1854–1912

Appendices (or should that be “appendices”?) make you look really clever, ‘cos it’s like you had more clever stuff to say than could be fitted into the main bit of your thesis. Yeah. So everyone should have at least three of them...

A.1. Anomalous Gauge Coupling Quartic Vertices Of Relevance in Vector Boson Scattering

The anomalous gauge couplings involving α_4 and α_5 arise in EFT through the addition of the following terms to the Lagrangian.

$$\text{Tr}(V^\mu V_\nu) \text{Tr}(V^\nu V_\mu) \text{ and } [\text{Tr}(V^\mu V_\mu)]^2 \quad (\text{A.1})$$

Where V_μ is defined in the following way.

$$V_\mu = \Sigma (D_\mu \Sigma)^\dagger \quad (\text{A.2})$$

and Σ , the Higgs field matrix, is defined as.

$$\Sigma = \exp\left(-\frac{i}{v}\mathbf{w}\right) \quad (\text{A.3})$$

Where $\mathbf{w} = w^a \sigma^a$. w^a are the ... and σ^a are the Pauli spin matrices. The covariant derivative of the Higgs field matrix is

$$D_\mu \Sigma = \left(\partial_\mu + \frac{ig}{2} W_\mu - \frac{ig'}{2} B_\mu \sigma^3 \right) \Sigma \quad (\text{A.4})$$

For clarity consider the unitarity gauge where $\mathbf{w} = 0$, which implies $\Sigma = 1$. In this gauge V_μ takes the following form.

$$\begin{aligned} V_\mu &= \frac{i}{2} (g W_\mu^i \sigma^i - g' B_\mu \sigma^3) = \frac{i}{2} \begin{pmatrix} g W_\mu^3 - g' B_\mu & g(W_\mu^1 - iW_\mu^2) \\ g(W_\mu^1 + iW_\mu^2) & -g W_\mu^3 + g' B_\mu \end{pmatrix} \\ &= \frac{i}{2} \begin{pmatrix} \sqrt{g^2 + g'^2} Z_\mu & g\sqrt{2} W_\mu^+ \\ g\sqrt{2} W_\mu^- & \sqrt{g^2 + g'^2} Z_\mu \end{pmatrix} \end{aligned}$$

Where the relationship between the mass and gauge symmetry basis are as follows.

$$W_\mu^+ = \frac{1}{\sqrt{2}} (W_\mu^1 - iW_\mu^2) \quad (\text{A.5})$$

$$W_\mu^- = \frac{1}{\sqrt{2}} (W_\mu^1 + iW_\mu^2) \quad (\text{A.6})$$

$$Z_\mu = c_w W_\mu^3 - s_w B_\mu \quad (\text{A.7})$$

$$A_\mu = s_w W_\mu^3 + c_w B_\mu \quad (\text{A.8})$$

With $c_w = \frac{g}{\sqrt{g^2 + g'^2}}$ and $s_w = \frac{g'}{\sqrt{g^2 + g'^2}}$. Consider the expansion of the terms to be included in the Lagrangian.

$$V^\mu V_\nu = \frac{-1}{4} \begin{pmatrix} \sqrt{g^2 + g'^2} Z^\mu & g\sqrt{2}W^{+\mu} \\ g\sqrt{2}W^{-\mu} & \sqrt{g^2 + g'^2} Z^\mu \end{pmatrix} \begin{pmatrix} \sqrt{g^2 + g'^2} Z_\nu & g\sqrt{2}W_\nu^+ \\ g\sqrt{2}W_\nu^- & \sqrt{g^2 + g'^2} Z_\nu \end{pmatrix} \quad (\text{A.9})$$

$$\text{Tr}[V^\mu V_\nu] = \frac{-1}{2}((g^2 + g'^2)Z^\mu Z_\nu + g^2 W^{+\mu} W_\nu^- + g^2 W^{-\mu} W_\nu^+) \quad (\text{A.10})$$

$$\text{Tr}[V^\mu V_\nu] \text{Tr}[V_\mu V^\nu] = \frac{(g^2 + g'^2)^2}{4}(Z^\mu Z_\mu)^2 + g^2(g^2 + g'^2)(Z^\mu Z^\nu W_\mu^- W_\nu^+) \quad (\text{A.11})$$

$$+ \frac{g^4}{2}(W^{-\mu} W_\mu^+)^2 + \frac{g^4}{2}(W^{-\mu} W^{+\nu} W_\mu^- W_\nu^+) \quad (\text{A.12})$$

$$\text{Tr}[V^\mu V_\mu]^2 = \frac{(g^2 + g'^2)^2}{4}(Z^\mu Z_\mu)^2 + g^2(g^2 + g'^2)(Z^\mu Z^\nu W_\mu^- W_\nu^+) \quad (\text{A.13})$$

$$+ g^4(W^{-\mu} W_\mu^+)^2 \quad (\text{A.14})$$

These two terms change the cross section for the vector boson scattering processes at CLIC that involve $ZZ \rightarrow ZZ$, $W^+W^- \rightarrow ZZ$, $ZZ \rightarrow W^+W^-$ and $W^+W^- \rightarrow W^+W^-$.

$$\text{Z} \quad \text{Z} \quad \text{Z} \quad \text{Z} \subset (\alpha_4 + \alpha_5) \frac{(g^2 + g'^2)^2}{4} \quad (\text{A.15})$$

(A.16)

$$Z \rightarrow W + W \subset (\alpha_4 + \alpha_5)g^2(g^2 + g'^2)$$

(A.17)

$$Z \rightarrow W + W \rightarrow W + W \subset (\alpha_4 + 2\alpha_5)\frac{g^4}{2} \text{ and } \frac{g^4}{2}\alpha_4$$

A.2. χ^2 Contour Plots for Jet Algorithm Optimisation

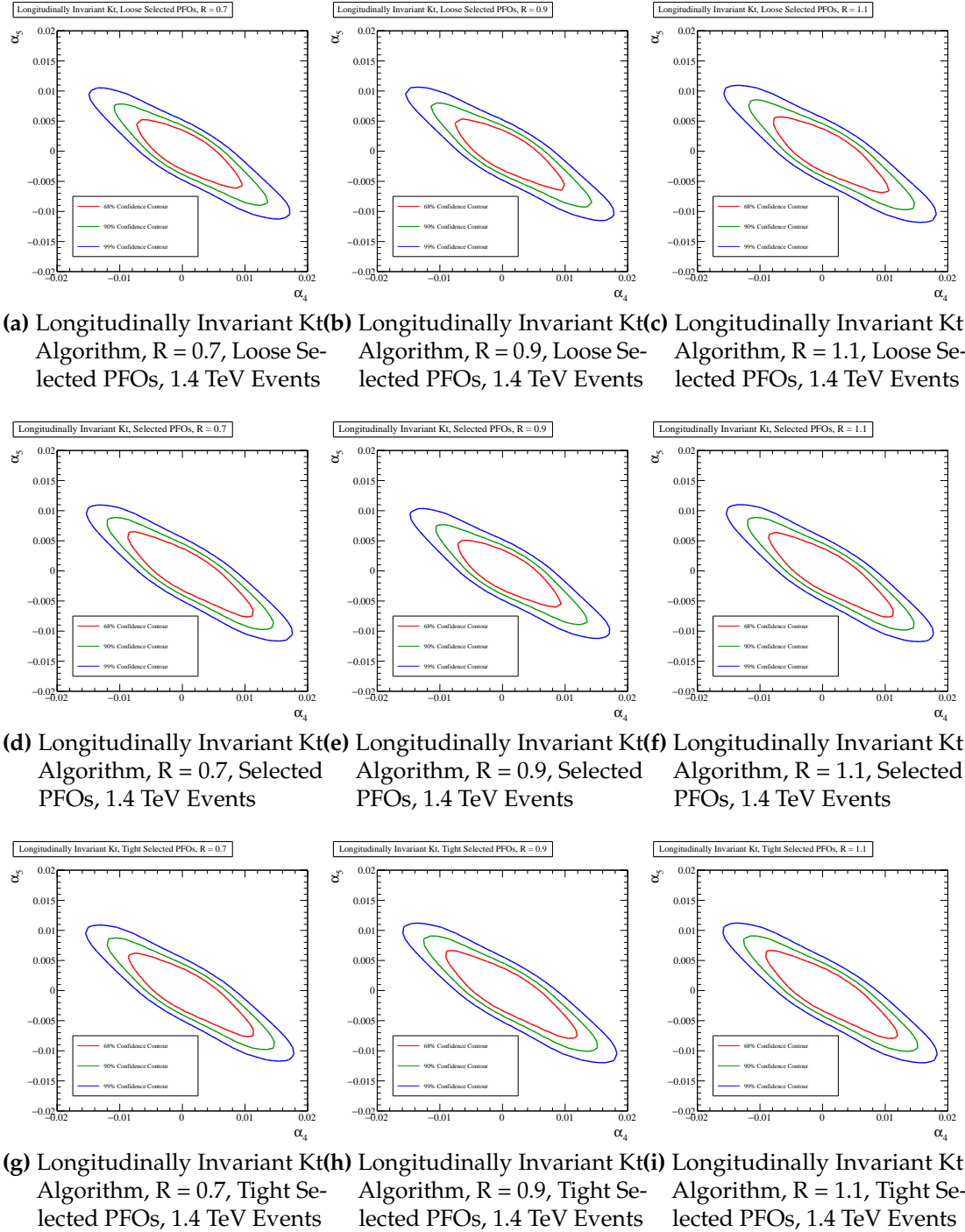


Figure A.1: χ^2 Sensitivity contours for the $qqqq\nu\nu$ final state arising from a fit to $\cos\theta_{\text{jets}}^*$ at 1.4 TeV for different values of jet reconstruction parameters.

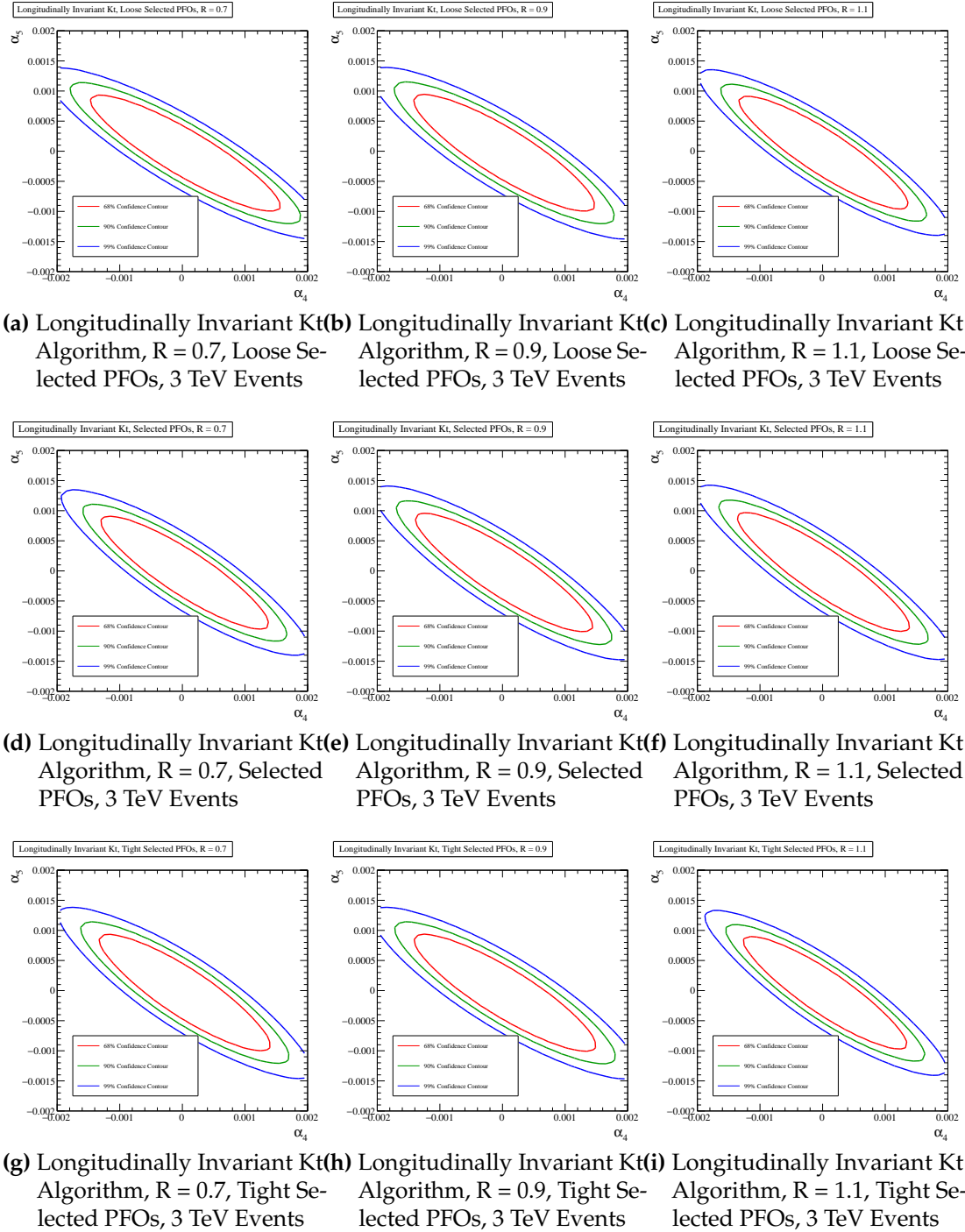


Figure A.2: χ^2 Sensitivity contours for the $qqqq\nu\nu$ final state arising from a fit to $\cos\theta_{\text{jets}}^*$ at 1.4 TeV for different values of jet reconstruction parameters.

Colophon

This thesis was made in L^AT_EX 2 _{ϵ} using the “hepthesis” class [3].

Bibliography

- [1] Toshinori Abe et al. The International Large Detector: Letter of Intent. 2010, 1006.3396.
- [2] S. Agostinelli et al. GEANT4: A Simulation toolkit. *Nucl. Instrum. Meth.*, A506:250–303, 2003.
- [3] Andy Buckley. The heptesis L^AT_EX class.
- [4] Matteo Cacciari, Gavin P. Salam, and Gregory Soyez. FastJet User Manual. *Eur. Phys. J.*, C72:1896, 2012, 1111.6097.
- [5] F. Gaede. Marlin and LCCD: Software tools for the ILC. *Nucl. Instrum. Meth.*, A559:177–180, 2006.
- [6] Andreas Hoecker, Peter Speckmayer, Joerg Stelzer, Jan Therhaag, Eckhard von Toerne, and Helge Voss. TMVA: Toolkit for Multivariate Data Analysis. *PoS*, ACAT:040, 2007, physics/0703039.
- [7] Wolfgang Kilian, Thorsten Ohl, and Jurgen Reuter. WHIZARD: Simulating Multi-Particle Processes at LHC and ILC. *Eur. Phys. J.*, C71:1742, 2011, 0708.4233.
- [8] Lucie Linssen, Akiya Miyamoto, Marcel Stanitzki, and Harry Weerts. Physics and Detectors at CLIC: CLIC Conceptual Design Report. 2012, 1202.5940.
- [9] J. S. Marshall, A. M^Ãajnnich, and M. A. Thomson. Performance of Particle Flow Calorimetry at CLIC. *Nucl. Instrum. Meth.*, A700:153–162, 2013, 1209.4039.
- [10] P. Mora de Freitas and H. Videau. Detector simulation with MOKKA / GEANT4: Present and future. In *Linear colliders. Proceedings, International Workshop on physics and experiments with future electron-positron linear colliders, LCWS 2002, Seogwipo, Jeju Island, Korea, August 26-30, 2002*, pages 623–627, 2002.
- [11] Mauro Moretti, Thorsten Ohl, and Jurgen Reuter. O'Mega: An Optimizing matrix

- element generator. 2001, hep-ph/0102195.
- [12] B. Pilicer, Helmut Burkhardt, Laurent Gatignon, Andrea Latina, Ercan Pilicer, Daniel Schulte, İlhan Tapan, and Rogelio Tomás. Study of Muon Backgrounds in the CLIC Beam Delivery System. In *Proceedings, 6th International Particle Accelerator Conference (IPAC 2015): Richmond, Virginia, USA, May 3-8, 2015*, page TUPTY032, 2015.
 - [13] András Sailer. *Radiation and Background Levels in a CLIC Detector due to Beam-Beam Effects*. PhD thesis, CERN, 2012-05-09.
 - [14] Torbjorn Sjostrand, Stephen Mrenna, and Peter Z. Skands. PYTHIA 6.4 Physics and Manual. *JHEP*, 05:026, 2006, hep-ph/0603175.
 - [15] M. A. Thomson. Particle Flow Calorimetry and the PandoraPFA Algorithm. *Nucl. Instrum. Meth.*, A611:25–40, 2009, 0907.3577.
 - [16] Z. Was. TAUOLA the library for tau lepton decay, and KKMC / KORALB / KORALZ /... status report. *Nucl. Phys. Proc. Suppl.*, 98:96–102, 2001, hep-ph/0011305. [,96(2000)].

List of figures

2.1.	Event weights from Whizard for 1.4TeV $\nu\nu\text{qqqq}$ final state events.	10
2.2.	Reconstructed invariant masses for different choices of jet algorithm for 1.4 TeV $\nu\nu\text{qqqq}$ events.	15
2.3.	χ^2 sensitivity distributions for the $\text{qqqq}\nu\nu$ final state arising from a fit to $\cos\theta_{\text{jets}}^*$ at 1.4 TeV for the optimal jet reconstruction parameters.	17
2.4.	Distribution of variables cut on in the preselection at 1.4 TeV.	22
2.5.	Impact of preselection and MVA on the reconstructed invariant mass of the bosons arising from jet pairing at 1.4 TeV.	25
2.6.	Sensitivity of $\cos\theta_{\text{jets}}^8$ to the anomalous gauge couplings α_4 and α_5 at 1.4 and 3 TeV.	28
2.7.	Sensitivity of $\cos\theta_{\text{Bosons}}^8$ to the anomalous gauge couplings α_4 and α_5 at 1.4 and 3 TeV.	28
2.8.	Event weights from Whizard for 1.4TeV $\nu\nu\text{qqqq}$ final state events with interpolated surface.	30
2.9.	χ^2 sensitivity distributions at 1.4 TeV arising from a fit to $\cos\theta_{\text{jets}}^*$. Results include the effect of backgrounds after the application of preselection and MVA.	32
2.10.	Comparison of various distributions between samples used in this analysis and the official CLIC samples for the $\nu\nu\text{qqqq}$ final state at 3 TeV.	33
2.11.	Reconstructed invariant masses for different choices of jet algorithm for 3 TeV $\nu\nu\text{qqqq}$ events.	33
2.12.	Distribution of variables cut on in the preselection at 3 TeV.	36

- 2.13. χ^2 sensitivity distributions for the $qqqq\nu\nu$ final state arising from a fit to $\cos\theta_{\text{jets}}^*$ at 3 TeV for the optimal jet reconstruction parameters. 39
- A.1. χ^2 Sensitivity contours for the $qqqq\nu\nu$ final state arising from a fit to $\cos\theta_{\text{jets}}^*$ at 1.4 TeV for different values of jet reconstruction parameters. 45
- A.2. χ^2 Sensitivity contours for the $qqqq\nu\nu$ final state arising from a fit to $\cos\theta_{\text{jets}}^*$ at 1.4 TeV for different values of jet reconstruction parameters. 46

List of tables

2.1.	Cross sections of signal and background processes at 1.4 TeV	11
2.2.	Cross section for selected processes for given value of α_4 and α_5 at 1.4 TeV. .	12
2.3.	The efficiency of isolated lepton finding at 1.4 TeV for the $\nu\nu\text{qqqq}$ and $l\nu\text{qqqq}$ final states.	18
2.5.	Number of events passing the various cuts applied in the preselection at 1.4TeV	23
2.6.	Number of events passing the MVA selection at 1.4TeV.	26
2.7.	Selection summary at 1.4TeV.	27
2.9.	Cross section for selected processes for given value of α_4 and α_5 at 3 TeV. .	34
2.10.	Number of events passing the various cuts applied in the preselection at 3 TeV.	35
2.11.	Number of events passing the MVA selection at 3 TeV.	37
2.12.	Selection summary at 3 TeV.	38
2.13.	1σ precision on measurement of α_4 for different jet reconstruction pa- rameters considering pure signal at 3 TeV.	40
2.14.	1σ precision on measurement of α_5 for different jet reconstruction pa- rameters considering pure signal at 3 TeV.	40